Loss of NR5A1 in mouse Sertoli cells after sex determination changes cellular identity and induces cell-death by anoikis

Sirine Souali-Crespo, Diana Condrea, Nadège Vernet, Betty Feret, Muriel Klopfenstein, Erwan Grandgirard, Violaine Alunni, Marie Cerciat, Matthieu Jung, Chloé Mayère, et al.

▶ **To cite this version:**

Sirine Souali-Crespo, Diana Condrea, Nadège Vernet, Betty Feret, Muriel Klopfenstein, et al.. Loss of NR5A1 in mouse Sertoli cells after sex determination changes cellular identity and induces cell-death by anoikis. Development (Cambridge, England), 2023, Development (cambridge, England), 150 (24), pp.dev201710. 10.1242/dev.201710 . hal-04341919

HAL Id: hal-04341919
https://hal.science/hal-04341919

Submitted on 13 Dec 2023

HAL is a multi-disciplinary open access archive for the deposit and dissemination of scientific research documents, whether they are published or not. The documents may come from teaching and research institutions in France or abroad, or from public or private research centers.

L'archive ouverte pluridisciplinaire **HAL**, est destinée au dépôt et à la diffusion de documents scientifiques de niveau recherche, publiés ou non, émanant des établissements d'enseignement et de recherche français ou étrangers, des laboratoires publics ou privés.

Distributed under a Creative Commons Attribution 4.0 International License

Loss of NR5A1 in mouse Sertoli cells after sex determination changes cellular identity and induces cell-death by anoikis

Sirine Souali-Crespo[1], Diana Condrea[1], Nadège Vernet[1], Betty Féret[1], Muriel Klopfenstein[1], Erwan Grandgirard[1,2], Violaine Alunni[1,3], Marie Cerciat[1,3], Matthieu Jung[1,3], Chloé Mayere[4], Serge Nef[4], Manuel Mark[1,5], Frédéric Chalmel[6,*], and Norbert B. Ghyselinck[1,*,‡]

[1]Institut de Génétique et de Biologie Moléculaire et Cellulaire (IGBMC), Département de Génétique Fonctionnelle et Cancer, Centre National de la Recherche Scientifique (CNRS UMR7104), Institut National de la Santé et de la Recherche Médicale (INSERM U1258), Université de Strasbourg (UNISTRA), 1 rue Laurent Fries, BP-10142, F-67404 Illkirch Cedex, France
[2]Imaging Center, IGBMC, F-67404 Illkirch Cedex, France
[3]GenomEast Platform, France Génomique consortium, IGBMC, 1 rue Laurent Fries, F-67404 Illkirch Cedex, France
[4]Department of Genetic Medicine and Development, Faculty of Medicine, University of Geneva, Geneva, Switzerland
[5]Service de Biologie de la Reproduction, Hôpitaux Universitaires de Strasbourg (HUS), France
[6]Univ Rennes, EHESP, Inserm, Irset (Institut de recherche en santé, environnement et travail) - UMR_S 1085, F-35000 Rennes, France

*These authors contributed equally to this work
‡Corresponding author: norbert@igbmc.fr; Tel: +33 388 655 674; Fax: +33 388 653 201

Author Contributions

SSC, MM and NBG conceptualized and designed the study. SSC and DC performed all the experiments. BF and MK provided technical and material support. EG contributed to image analysis. SSC, VA, MC, MJ and FC performed the scRNA-seq experiment and analyzed data. CM and SN provided datasets for the mouse gonad atlas. SSC, NV, MM, FC and NBG analyzed all experiments, managed the overall study, wrote the manuscript, and supervised its preparation and submission. NV, MM, FC and NBG acquired funding for this research.

Keywords: gonad, integrin, Leydig, mutant, testis, SF-1.

© 2023. Published by The Company of Biologists Ltd.
This is an Open Access article distributed under the terms of the Creative Commons Attribution License (http://creativecommons.org/licenses/by/4.0), which permits unrestricted use, distribution and reproduction in any medium provided that the original work is properly attributed

Development • Accepted manuscript

Summary statement

Loss of NR5A1 after the sex-determination period causes Sertoli cells to revert to supporting progenitor-like cells and transdifferentiate into pre-granulosa-like cells that die by a *Trp53*-independent mechanism.

Abstract

To investigate the role of the nuclear receptor NR5A1 in testis after sex determination, we have analyzed mice lacking NR5A1 in Sertoli cells (SC) from embryonic day (E) 13.5 onwards. Ablation of *Nr5a1* impairs the expression of genes characteristic of the SC identity (e.g., *Sox9*, *Amh*), causes SC death from E14.5 through a *Trp53*-independent mechanism related to anoikis, and induces disorganization of the testis cords. Together, these effects cause germ cells to enter meiosis and die. Single-cell RNA-sequencing experiments revealed that NR5A1-deficient SC change their molecular identity: some acquire a “pre-granulosa-like” identity, while other revert to a “supporting progenitor-like” cell identity, most of them being “intersex” because they express both testicular and ovarian genes. Fetal Leydig cells (LC) do not display significant changes, indicating that SC are not required beyond E14.5 for their emergence or maintenance. In contrast, adult LC were absent from the postnatal testes. In addition, adult mutant males display persistence of Müllerian duct derivatives, decreased anogenital distance and reduced penis length, which can be explained by the loss of AMH and testosterone synthesis due to SC failure.

Introduction

In humans, a group of defects known as developmental sex disorders (DSD) are caused by mutations in certain genes regulating gonad development. Critically, these disorders provide an important system for understanding the molecular mechanisms that underpin cell differentiation (Eggers et al., 2014). Among the genes responsible for DSD is *NR5A1* (Fabbri-Scallet et al., 2020), which encodes the orphan nuclear receptor NR5A1, a transcription factor that is expressed at the stage when cells acquire a fate of either adrenal or gonadal primordium (Morohashi et al., 2013). Consistent with a role in DSD, NR5A1 has been reported to regulate proliferation, survival and differentiation of somatic progenitor cells through specific gene expression (Morohashi et al., 2020).

These somatic progenitors play a critical role in sex determination. Both testes and ovaries originate from a bipotential gonad that contains the primordial germ cells (GC) and the early somatic progenitors. Around embryonic day (E) 11.5 in the mouse, it is these

Development • Accepted manuscript

somatic progenitors that first undergo sex-specific cell differentiation into bipotential supporting progenitors (supP), and then into either pre-Sertoli cells (SC) in the testis upon SRY/SOX9 expression, or into pre-granulosa (pGr) cells in the ovary upon WNT/CTNNB1 signaling stabilization (Nef et al., 2019). The sex-specific fate decision then propagates to the GC and to other somatic lineages in the testis, including the steroidogenic Leydig cells (LC) which, in turn, drive the acquisition of primary and secondary sexual characters at later stages of development, through hormone secretion (Yao et al., 2015; Rotgers et al., 2018; Nef et al., 2019).

Knock-out of *Nr5a1* in the mouse results in regression of the gonads by E11.5 due to apoptosis of somatic cells, and agenesis of the adrenal glands (Luo et al., 1994). From E11.5, NR5A1 and SRY are expressed in the bipotential supP cells of the male gonad, where they upregulate SOX9 expression, initiating thereby pre-SC and ultimately SC differentiation (Sekido and Lovell-Badge, 2008; Rotgers et al., 2018; Nef et al., 2019). Once specified, the SC start forming cords by enclosing GC as early as E12.5 in the mouse (Cool et al., 2012), providing them with a specialized environment that promotes their survival and orchestrates their differentiation (Griswold, 2018). SC also allow the differentiation of fetal LC through paracrine Desert Hedgehog (DHH) signaling (Bitgood et al., 1996), and produce high levels of anti-Müllerian hormone (AMH) under the control of NR5A1 and SOX9, which triggers the regression of the Müllerian duct normally giving rise to the female genitalia (Josso and Picard, 2022).

Since gonads are absent in *Nr5a1*-null mice (Luo et al., 1994), studying the cell-specific role of NR5A1 in the developing testis required analysis of mice bearing tissue-targeted mutations. Here we have analyzed the outcome of *Nr5a1* ablation in SC from E13.5 onwards. We show that loss of NR5A1 from this stage causes some SC to revert to a supP cell-like state, some other to sexually transdifferentiate into female somatic pGr cells, and all of them to die by a *Trp53*-independent mechanism related to anoikis.

Results

Deletion of *Nr5a1* in Sertoli cells

To achieve *Nr5a1* ablation in SC after sex determination, we introduced the *Plekha5*$^{Tg(AMH\text{-}cre)1Flor}$ transgene (Lécureuil et al., 2002) in mice bearing *lox*P-flanked alleles of *Nr5a1* and a Cre-dependent yellow fluorescent protein (YFP) reporter transgene (Srinivas et al., 2001). Cre-mediated recombination was assessed by immunohistochemistry (IHC) using antibodies recognizing the YFP. Surprisingly, YFP was detected in all SC of embryonic day (E) 12.5 gonads (arrows, Fig. 1A,B), indicating Cre-mediated excision occurred earlier than

Development • Accepted manuscript

anticipated (Lécureuil et al., 2002). However, the NR5A1 protein was still detected in SC at E12.5 (Fig. 1A,B). It was lost in the mutant testis at E13.5 (Fig. 1D), but maintained in the control testis (Fig. 1C). Importantly, NR5A1 was still detected in the nuclei of LC, identified by their expression of the steroid 3 beta-hydroxy-steroid dehydrogenase type 1 (HSD3B1), in both control and mutant testes (Fig. 1E,F). Thus, NR5A1 was lost selectively in SC from E13.5 onwards, generating males hereafter referred to as *Nr5a1*$^{SC-/-}$ mutants.

Ablation of Nr5a1 *in SC impairs expression of SOX9, SOX8, SOX10 and AMH*

As NR5A1 regulates the expression of *Amh* and *Sox9* genes (De Santa Barbara et al., 1998; Sekido and Lovell-Badge, 2008), we tested expression of these proteins by IHC. Both AMH and SOX9 were detected at normal levels at E12.5 (Fig. 2A,B,G,H). Their expression decreased progressively between E13.5 and E14.5 in *Nr5a1*$^{SC-/-}$ mutant testes (Fig. 2C-F,I-L). The expression of SOX8 and SOX10 was also decreased (Fig. S1). Accordingly, the steady state levels of *Amh*, *Sox9* and *Sox8* mRNAs was decreased in *Nr5a1*$^{SC-/-}$ testes (Fig. 2S). The level of prostaglandin D2 synthase (*Ptgds*) mRNA, a SOX9 target-gene (Wilhelm et al., 2007), was also reduced in *Nr5a1*$^{SC-/-}$ testes. This finding may explain the cytoplasmic, instead of the nuclear, localization of SOX9 in some mutant SC (compare insets, Fig. 2K,L) because prostaglandin D2, the end product of PTGDS, is required for SOX9 nuclear translocation (Malki et al., 2005).

In parallel, we analyzed the expression of GATA4 and WT1 transcription factors, which are important for *Amh* expression and SC differentiation (Trembaly and Viger, 1999; Buganim et al., 2012). Both were detected at similar levels in SC nuclei of control and mutant testes, from E12.5 to E14.5 (Fig. 2M-R; Fig. S1).

Ablation of *Nr5a1* in SC induces disorganization of the testis cords

On histological sections at E14.5, the majority of *Nr5a1*$^{SC-/-}$ seminiferous cords displayed reduced diameters, as well as poorly defined and discontinuous contours (Fig. 3E). At E15.5, the cords had almost completely disappeared (Fig. 3F). Such irregularities were never observed in the control testes (Fig. 3A,B).

To visualize seminiferous cord basement membranes, we analyzed the expression of collagen type IV (COL-IV) by IHC. At E14.5, COL-IV surrounded the entire periphery of all cords in control testes (yellow border, Fig. 3C). In *Nr5a1*$^{SC-/-}$ testes, COL-IV was greatly reduced and even absent from the periphery of many cords (arrows, Fig. 3G), in areas corresponding to regions where SOX9 expression was also lost (arrowheads, Fig. 3H). Since

Development • Accepted manuscript

Col4a1 and *Col4a2* are regulated by SOX9 (Sumi et al., 2007), it is proposed that loss of SOX9 in NR5A1-deficient SC resulted in loss of COL-IV and altered basement membrane, which, in turn, disorganized the cord structure. Knowing that testis cord formation and vasculature are closely linked (Brennan et al., 2003), the question aroused whether the vasculature was affected in *Nr5a1*$^{SC-/-}$ testes. We show that it was normal, at least until E14.5 (Fig. S2).

NR5A1-deficient SC die through a TRP53-independent mechanism

By virtue of YFP expression we could quantify the surface occupied by SC (green pixels) relative to the whole testis surface (Fig. 4A-D). At E14.5, this ratio was about 30% lower in mutant than in control testes [28.3 ± 3.8 (n=5) versus 37.9 ± 2.5 (n=5), respectively; $p < 0.01$]. This suggested that NR5A1-deficient SC had either silenced expression of YFP or had disappeared from the testis. If YFP expression was silenced, the Cre-recombined *Nr5a1* allele (L-) should be present in the testis at birth. It should no longer be detected if SC were lost. As a matter of fact, PCR analysis of genomic DNA showed that the L– allele was not present to any significant degree in *Nr5a1*$^{SC-/-}$ mutants (Fig. S3A), indicating that NR5A1-deficient SC were actually lost from the mutant testis. Consistent with mutant SC elimination, numerous cells displaying features of SC (i.e., located at the periphery of the testis cords, amongst GATA4-expressing SC) were TUNEL-positive in E14.5 *Nr5a1*$^{SC-/-}$ testis (arrowheads, Fig. 4E,F). This indicates that NR5A1-deficient SC died progressively.

Previously, ablation of *Nr5a1* in SC was proposed to increase phosphorylation of TRP53 and to induce apoptosis (Anamthathmakula et al., 2019). However, TRP53 could not be detected by IHC in SC at E14.5 (Fig. 4G,H). Therefore, to test whether TRP53 was involved in SC-death we set up a functional assay. We introduced conditional alleles of *Trp53* (Jonkers et al., 2001) into *Nr5a1*$^{SC-/-}$ mutants carrying the YFP reporter transgene. Efficient ablation of *Trp53* was assessed by PCR on genomic DNA extracted from FACS-purified, YFP-positive, SC (Fig. S3B). Contrary to the expectations, both *Nr5a1*$^{SC-/-}$ and *Nr5a1*$^{SC-/-}$;*Trp53*$^{SC-/-}$ mutant testes at E14.5 displayed identical defects, including the loss of SOX9 expression and the decreased number of SC (Fig. 4I-J, compare with 3A). In addition, both *Nr5a1*$^{SC-/-}$ and *Nr5a1*$^{SC-/-}$;*Trp53*$^{SC-/-}$ mutant testes lacked SC-surrounded seminiferous tubules at postnatal day 15 (PND15). Instead, they contained interstitial cells, including HSD3B1-positive fetal LC (Fig. 4K-P). This indicates that TRP53 was not necessary for NR5A1-deficient SC to die. At adulthood, none of the interstitial of cells expressed the adult LC-specific marker BHMT (Sararols et al., 2021) in *Nr5a1*$^{SC-/-}$ testes, suggesting that this cell-type was unable to emerge during postnatal testis development (Fig. 4Q-S). Altogether,

Development • Accepted manuscript

these data indicate that NR5A1-deficient SC died in a TUNEL-positive, but TRP53-independent manner, resulting in a postnatal testis containing fetal but not adult LC.

Nr5a1$^{SC-/-}$ adult males exhibit retention of Müllerian duct derivatives

We analyzed the outcome of the loss of SC and AMH production in *Nr5a1*$^{SC-/-}$ mutants at PND60. The males were all sterile and had a shorter anogenital distance (AGD) index [0.30 ± 0.03 mm/g of body weight in mutants (n=16), versus 0.36 ± 0.02 mm/g in controls (n=17); $p < 0.001$] (Fig. 5A,C). At autopsy (n = 8), they displayed normal derivatives of the Wolffian ducts (e.g., epididymis, vas deferent, seminal vesicle) and the urogenital sinus (i.e., prostatic lobes) (Fig. 5E,F). However, they also displayed Müllerian duct derivatives (Fig. 5F-H), namely a vagina, a uterine body and bilateral uterine horns, which were either incomplete and truncated (6 out of 8), or complete on one side (2 out of 8). Histological analyses revealed that the uterine body and vagina displayed a columnar epithelium (Fig. 5I) and a stratified squamous epithelium (Fig. 5J), as anticipated for these female organs.

In addition, *Nr5a1*$^{SC-/-}$ males displayed 40% lighter seminal vesicles [4.71 ± 1.66 mg/g of body weight in mutants (n=17), versus 7.43 ± 1.22 mg/g in controls (n=16); $p < 0.05$] and 10% shorter penis bones [6.7 ± 0.4 mm in mutants (n=17), versus 7.5 ± 0.3 mm in controls (n=16); $p < 0.05$) (Fig. 5B,D). As AGD, seminal vesicle growth and penis bone length vary as a function of androgen exposure (Welsh et al., 2014), we tested blood testosterone levels. They were comparable at birth [0.25 ± 0.17 ng/ml in mutants (n=10), versus 0.22 ± 0.10 ng/ml in controls (n=10); $p = 0.59$], and at PND60 [0.38 ± 0.17 ng/ml in controls (n=17), versus 0.43 ± 0.23 ng/ml in controls (n=16); $p = 0.68$], indicating normal testosterone production.

Transcriptomic signatures of cells in control and NR5A1-deficient testes

We then performed single-cell RNA sequencing (scRNA-seq) experiments using dissociated cell suspensions obtained from 12 control and 16 *Nr5a1*$^{SC-/-}$ whole testes at E13.5 and E14.5. After data processing and quality control, we assembled an atlas composed of 3,988 and 5,010 control and mutant testicular cells, respectively. On average, we detected 13,860 unique molecular indices (UMIs) and approximately 3,500 genes for each cell. The 8,998 testicular cells were partitioned into 23 cell clusters (termed C1-C23) and projected into a two-dimensional space (Fig. 6A; Table S1). Known marker genes of distinct cell-types were used to identify each cluster (Fig. S4).

Development • Accepted manuscript

Very few changes of gene expression were observed between control and *Nr5a1*$^{SC-/-}$ testes for endothelial, immune and perivascular cells. In Leydig, interstitial, coelomic epithelium and peritubular myoid (PTM) cells the expression of 59, 49 and 47 genes was significantly ($p < 0.05$) dysregulated (Table S2). Functional analysis revealed that downregulated genes were related to the ribosome biosynthesis in Leydig and interstitial cells, and epithelium development in coelomic epithelium and PTM cells (Fig. S5; Table S3). In GC, the expression of 636 genes was significantly dysregulated (Table S2), among these we found that *Stra8* and *Rec8* were upregulated, while *Nanos2* and *Piwil4* were downregulated (Fig. 6B). Processes such as DNA recombination, meiotic cell cycle and oocyte differentiation were identified among the GO terms associated with upregulated genes (Fig. S5; Table S3). Accordingly, we showed that GC in *Nr5a1*$^{SC-/-}$ testes at E14.5 and E15.5 were in the S-phase of the meiotic prophase, instead of becoming mitotically quiescent, as in the control situation (Fig. S6A-G). In addition, many GC of the *Nr5a1*$^{SC-/-}$ testes expressed meiotic proteins, such as STRA8, REC8 or H2AFX (Fig. S6H-O), and died (Fig. S6P-R).

Three clusters of SC were identified (C18, C19 and C21). The C18 cluster included both control and NR5A1-deficient SC (Fig. 6A) and had hallmarks of mitotic cells (Fig. S4B). The C19 and C21 clusters consisted almost exclusively of control and NR5A1-deficient SC, respectively (Fig. 6A). In total, 1,671 genes were significantly dysregulated in SC lacking NR5A1 (Table S2), amongst which *Amh*, *Ptgds* and *Sox9* were down, as anticipated (see above), while *Fst*, *Rspo1* and *Wnt4* were up (Fig. 6C). As for *Dmrt1*, its expression was reduced in SC and increased in GC of the *Nr5a1*$^{SC-/-}$ testes (Fig. 6M). We confirmed the dysregulated expression of some genes by IHC (Fig. 6D-K) or RT-qPCR (Fig. 6L), thereby validating thereby the scRNA-seq experiment. Based on the fact that *rete* testis cells express *Aldh1a3*, *Pax8* and *Nr5a1* (Mayère et al., 2022), cluster C20 was assigned the *rete* testis identity (Fig. S4). The cells in this cluster were organized as a continuum, starting from C19 with true SC (*Nr5a1*$^{+}$/*Yfp*$^{-}$/*Pax8*$^{-}$/*Aldh1a3*$^{-}$) and extending with *rete* cells (*Nr5a1*$^{+}$/*Yfp*$^{-}$/*Pax8*$^{+}$/*Aldh1a3*$^{+}$) derived from both control and *Nr5a1*$^{SC-/-}$ testes. Accordingly, IHC experiments showed that *rete* testis cells actually expressed ALDH1A3, PAX8 and NR5A1, but not YFP, in both control and *Nr5a1*$^{SC-/-}$ testes (Fig. S7). This can be explained by the fact that the *Plekha5*$^{Tg(AMH-cre)1Flor}$ transgene is not active in the *rete testis* cells (Teletin et al., 2019).

Development • Accepted manuscript

Death of NR5A1-deficient SC is associated to anoikis

Functional analysis of the differentially expressed genes (DEG) between control and NR5A1-deficient SC highlighted GO terms such as extracellular matrix (ECM), basement membrane, cell-substrate adhesion and integrin binding (Fig. S5; Table S3). Accordingly, the expression of genes involved in cell junction/adhesion (e.g., *Gja1*, *Jam2*, *Ptk2b*) and integrin signalling (e.g., *Itga6*) was reduced in mutant SC. As for ECM component genes, some were downregulated (e.g., *Col4a1*, *Col4a2*), while others (e.g., *Col3a1*, *Col5a2*, *Col6a6*, *Fn1*, *Fbln1*, *Mdk*, *Mgp*) were upregulated in mutant SC (Fig. 7A). Further searching for ligand-receptor interactions in our data set, we identified a dysregulated network related to integrin-dependent cell adhesion (Fig. S8). These findings indicate that NR5A1-deficient SC lost their appropriate cell-cell and cell-ECM, integrin-dependent, interactions, and are consistent with the basement membrane alteration described above (see Fig. 3). This raised the possibility that NR5A1-deficient SC die by detachment-induced cell-death (a.k.a., anoikis).

Anoikis is the induction of apoptosis in anchorage-dependent cells and it occurs upon loss of attachment to the ECM (Gilmore, 2005; Vachon, 2011). Indeed, functional analysis of overexpressed genes in NR5A1-deficient SC revealed regulation of cell-death and of apoptotic process among the altered functions (Fig. S5; Table S3). Furthermore, 26 of the 88 anoikis-related genes with a GeneCards score greater than 2.0 were deregulated in NR5A1-deficient SC (Fig. 7B; Table S4). Similar to apoptosis, anoikis leads to the activation of caspases, either through the intrinsic or the extrinsic apoptotic pathway. Therefore, the quantification of caspase 3 activity can serve as a marker of the anoikis cell-death process (Tedja et al., 2021). Using FACS-purified, YFP-positive SC at E13.5, we found that caspase 3 activity was indeed 4-fold higher in NR5A1-deficient than in control SC (Fig. 7C). In addition, using the mouse SC line MSC-1 as a surrogate model of control SC (McGuinness et al., 1994), we showed that SC survived when cultured *in vitro* on normal (uncoated) plates, but died when cultured on anchorage-resistant (hydrogel-coated) plates (Fig. 7D-H). Taken together these results indicate that SC normally rely on cell-ECM attachment to survive, and that this property is compromised when NR5A1 is lost.

Nr5a1 ablation alters the molecular identity of SC

The NR5A1-deficient SC in cluster C21 gained expression of *Wnt4*, *Fst* and *Rspo1* (Fig. 6C; Table S2), which are hallmarks of the fetal ovarian somatic cells (Eggers et al., 2014). This raised the question as to whether some SC had adopted a sex-reversed cell differentiation pathway. To test for this possibility, we compared our data with a reference atlas of embryonic and fetal gonadal cell transcriptomes ranging from E10.5 to E16.5

Development • Accepted manuscript

(Mayère et al., 2022). After processing this atlas with the pipeline that we used for our data set (Fig. S9), we mapped our data set to the reference atlas (Fig. 8A). Most of control and *Nr5a1*$^{SC-/-}$ cell clusters were predicted to correspond to clusters with identical or similar identities (Fig. 8B). Consistent with our expectation, cluster C20 was predicted to correspond best with *rete* testis cells (see above, Fig. S7). In addition, the majority of GC from control testes matched with E13.5 male GC in the atlas, whereas a large proportion of those from *Nr5a1*$^{SC-/-}$ testes matched with E13.5 female (i.e., meiotic) GC (Fig. 8C), as shown by IHC analyses (Fig. S6), thus validating the strategy in general. Most importantly, NR5A1-deficient SC (cluster C21) corresponded not only to E13.5 SC, but also to E16.5 pGr cells in the atlas (Fig. 8B,C). Thus, a fraction of NR5A1-deficient SC lost its identity, and acquired a pGr-like cell identity. Accordingly, GO term analysis assigned upregulated genes in NR5A1-deficient SC to the WNT signalling pathway, which is known to drive pGr cell differentiation in the fetal ovary (Chassot et al., 2014; Fig. S5; Table S3), and we observed expression of *Wnt4* and *Fst* mRNA in the seminiferous cords of *Nr5a1*$^{SC-/-}$ but not control testes (Fig. 8D-G). However, the process of sexual transdifferentiation remained abnormal, as IHC experiments showed no evidence of FOXL2 expression in the *Nr5a1*$^{SC-/-}$ mutant testes at E15.5 (Fig. 8H,I).

To test whether some SC had adopted a cellular identity corresponding to another cell type, we then mapped the somatic cells of our data set (Fig. S10) to the male somatic cells of the reference atlas (Fig. S11; Mayère et al., 2022). Again, control and most of *Nr5a1*$^{SC-/-}$ cells matched to cell types with the expected identities (Fig. 9A), with the notable exception of NR5A1-deficient SC, which matched to cell types such as E12.5 interstitial and E11.5 supP cells, in addition to SC and *rete* testis cells (Fig. 9B). This raised the possibility that some mutant SC might revert to somatic cells of an earlier developmental stage. Consistent with this idea, they expressed *Nr2f2* mRNA (arrowhead, Fig. S12A), and NR2F2 protein could be detected in some SC of *Nr5a1*$^{SC-/-}$ but not control testes (Fig. 9C,D). Interestingly, NR2F2 is a hallmark of bipotential supP cells (Stévant et al., 2019). To test whether NR2F2-deficient SC indeed reverted to “supP-like” cells, we inferred cell differentiation lineages and pseudo-time using the Slingshot method (Street et al., 2018). We obtained linear trajectories for each cell type, along which the majority of NR5A1-deficient SC were at the strating point of the SC differentiation pathway, where supP cells are located (arrowhead, Fig. 9E). Correspondingly, prediction of developmental stage and pseudo-time revealed that NR5A1-deficient SC matched to the E10-E12 stages, while control SC matched to the E13-E15 stages (Fig. 9F; Fig. S12B). This supported the idea that loss of *Nr5a1* shifts some SC to an earlier, “supP-like”, state of differentiation. However, out of the 605 *Nr2f2*-positive NR5A1-deficient SC, 174 (29%) which co-expressed the male-specific gene *Eif2s3y* (Stévant et al., 2019) could be assigned the “male supP-like” cell identity, 87 (14%) which co-expressed the

Development • Accepted manuscript

female-specific gene *Aldh1a2* (Stévant et al., 2019) could be assigned the “female supP-like” cell identity, and 276 (46%) were assigned an “intersex supP-like” cell identity because they co-expressed both *Eif2s3y* and *Aldh1a2* (Fig. 9G). Taken together, this indicated that loss of NR5A1 dedifferentiated SC into a heterogenous population, consisting of “pGr-like” cells, as well as male, female and intersex E10-E12 “supP-like” cells.

Ablation of *Nr5a1* does not alter ATP metabolism in SC

Previously, it was shown in adrenocortical cells cultured *in vitro* that suppression of NR5A1 reduces the production of the energy carriers adenosine triphosphate (ATP) and nicotinamide adenine dinucleotide phosphate (NADPH), and decreases the expression of genes involved in glucose metabolism (Baba et al., 2014). Consistent with this possibility, functional analysis of upregulated genes in NR5A1-deficient SC highlighted ATP metabolism and glycolysis / gluconeogenesis (Fig. S5; Table S3). However, while the expression of most of the genes involved in ATP synthesis was indeed increased by 20-50% in mutant SC (Fig. S13A), we found that ATP production was decreased by approximately 20%, although the difference was not statistically significant [$43.7^{e4} \pm 5.3^{e4}$ RFU in mutants (n=6), versus $35.3^{e4} \pm 8.1^{e4}$ RFU in controls (n=6); $p = 0.060$] (Fig. S13B). The association between reduced ATP production and increased gene expression may reflect the fact that SC were dying. Regarding the glycolysis pathway, the expression of most of the genes was increased by 20-30% in mutant SC (Fig. S13C), except that of *Hk1*, *Aldoa*, *Pgam1* and *Eno1*, which was decreased by 20- 40% (Fig. S13D). In this context, it is worth noting that these four genes contain NR5A1-responsive elements (Baba et al., 2014), suggesting that their reduced expression was directly linked to the loss of NR5A1. We did not test whether these changes caused an increase or a decrease of glycolysis. The fact that the NR5A1-deficient SC were dying added a confounding factor, that may affect the correct interpretation of the result as was the case for ATP production.

Discussion

Understanding developmental sex disorders (DSD) provides tools and insights into more general developmental processes. In this study, we have investigated the role of the DSD gene *Nr5a1* in SC after the sex determination period. Our study shows that SC lacking NR5A1 from E13.5 lose the expression of genes that define or maintain SC identity, illustrating that NR5A1 plays a primary role in these processes. Among the genes whose expression is reduced in SC lacking NR5A1 is *Dmrt1*, a pioneer factor that enables SOX9 binding and plays a critical role in post-natal male sex maintenance (Matson et al., 2011; Lindeman et al., 2021). However, since *Dmrt1* knockout does not alter SC fate until PND7

Development • Accepted manuscript

(Murphy et al., 2022), it is unlikely that this gene participates to the sex reversal displayed by *Nr5a1*$^{SC-/-}$ males. Most of the defects displayed by *Nr5a1*$^{SC-/-}$ testes are schematized in Fig. 10. The set of abnormalities generated by ablation of *Nr5a1* at distinct time-points in other studies are recapitulated in Table S5.

NR5A1-deficient SC change their cellular identity

In the absence of NR5A1, some SC gain expression of genes characteristic of the "supP-like" lineage (e.g., *Nr2f2*), and some undergo sexual transdifferentiation into "pGr-like" cells. In general, there are two possible scenarios for transdifferentiation: either the cells first dedifferentiate into an intermediate state of limited potency and then redifferentiate into another cell type, or the cells transform directly into another cell type. The first scenario is not known to occur in other mouse genetic models of sexual transdifferentiation (Jimenez et al., 2021). In the case of *Foxl2* post-natal ablation, transdifferentiation of granulosa cells into SC is immediate (Uhlenhaut et al., 2009), favoring the second scenario. In the present case, we cannot claim that the NR5A1-deficient SC first revert to the "supP-like" state, which would correspond to the intermediate state, before acquiring the "pGr-like" state. It should be noted, however, that the "supP-like" cells do not revert to a true bipotential state, as defined previously (Stévant et al., 2019). A large proportion of them do not follow a strict male-female binary distribution. These cells express both male- and female-specific genes, and are therefore qualified as "intersex supP-like". Some of them retain a male-oriented identity, while some other displays a female-oriented identity. Such a distribution, coupled with the presence of "pGr-like" cells, allows to propose a scenario according to which NR5A1-deficient SC could first dedifferentiate into "male-oriented supP-like" cells, which then become "intersex supP-like cells" because they lose the expression of male-promoting genes and express female-promoting genes, which progressively become "female-oriented supP-like" cells, which finally differentiate into "pGr-like" cells.

Interestingly, ablation of *Nr5a1* at an earlier stage than in the present study (i.e., from E12.5) allows SC to acquire a FOXL2-positive granulosa cell identity, resulting in male-to-female sex reversal (Ikeda et al., 2021). This indicates that SC devoid of NR5A1 from E12.5 can fully transdifferentiate into granulosa cells, whereas those that lose NR5A1 from E13.5 (our study) are no longer licensed to do so. Conversely, when ablation of *Nr5a1* occurs at a later stage than in the present study (i.e., from E14.5), SC do not change identity at all, but a proportion of them die by MDM2/TRP53-dependent apoptosis (Anamthathmakula et al., 2019). In the present study, ablation of *Nr5a1* at E13.5 causes SC to revert to "supP-like" and "pGr-like" cells that do not reach a state of full sexual transdifferentiation as they remain

Development • Accepted manuscript

FOXL2-negative. Thus, the earlier NR5A1 is lost in SC after sex determination, the greater is the cellular plasticity that SC retain, suggesting that *Nr5a1* locks SC identity over time.

Sertoli cells lacking NR5A1 from E13.5 die by anoikis

Cells sense their position and maintain their adhesion through specific interactions with the ECM. This plays a major role in the regulation of various processes, including cell survival and maintenance of seminiferous cord integrity (Matoba et al., 2018; Barrionuevo et al., 2009; Georg et al., 2012; Chen et al., 2013). This function is mediated by integrins, which are the cell-membrane receptors that interact with components of the ECM. They recruit nonreceptor tyrosine focal adhesion kinases (FAK), which are activated in response to adhesion (Lu and Rounds, 2012). Disruption or loss of integrin-ECM adhesion impairs cell survival, and often leads to detachment-induced cell death, a process also known as anoikis (Gilmore, 2005; Vachon, 2011). Physiologically, anoikis serves to prevent detached cells from adhering to an ECM other than that to which they were assigned, or to prevent cells from migrating to wrong locations. Similar to apoptosis, anoikis leads to DNA fragmentation and activation of caspase 3 (Tedja et al., 2021), but unlike apoptosis, anoikis does not require the involvement of TRP53 (McGill et al., 1997).

We report here that the expression of *Itga6*, an integrin subunit critical for fetal testis organization (Fröjdman and Pelliniemi, 1994), and *Ptk2b*, a member of the FAK family (Beverdam et al., 2010) is reduced in NR5A1-deficient SC. We also show that the adhesion molecules and ECM expressed by NR5A1-deficient SC are profoundly altered, with some of the acquired protein being characteristic of pGr cells (e.g., *Col18a1*, *Fn1*, *Nid2* and *Dcn*; Table S2) (Piprek et al., 2018). Thus, it is conceivable that all these changes disrupt the anchorage of SC to the ECM and induce death by anoikis, thereby altering the integrity of the testis cord epithelium. Consistent with this proposal we show that SC lacking NR5A1 display the hallmarks of anoikis: they express many anoikis-related genes, they are TUNEL-positive (i.e., their DNA is fragmented), they have increased caspase 3 activity, and they die even when TRP53 is absent. In addition, using the MSC-1 cell line as a surrogate model for SC, we show that impairment of cell attachment *in vitro* induces SC death.

Interestingly, when NR5A1 is deleted from E12.5, SC do not die but transdifferentiate into granulosa cells (Ikeda et al., 2021). When NR5A1 is lost from E13.5, SC change their identity to “supP-like” and “pGr-like” cells and die by anoikis (our study). When SC lose NR5A1 later than E14.5, many of them survive giving rise to testes with well-defined seminiferous tubules at adulthood, but some others die by a TRP53-dependent mechanism

Development • Accepted manuscript

(Anamthathmakula et al., 2019). This observation suggests that the ability of SC to die, and the underlying mechanism, depend on NR5A1 and on the cell differentiation status.

Death of the NR5A1-deficient SC affects genital tract development

The action of AMH on regression Müllerian ducts in males proceeds rostro-caudally and begins as early as E13.5 (Staack et al., 2003; Mullen and Behringer, 2014). As *Amh* expression is lost only from E14.5 in *Nr5a1*$^{SC-/-}$ mutants, AMH production starts normally and then gradually decreases to zero after E14.5. It is therefore not surprising that the rostral part of the Müllerian ducts regresses normally, making their derivatives (oviducts, anterior portions of the uterine horns) absent in the mutants, while the caudal part of the Mullerian ducts persists beyond E14.5, being at the origin of the posterior portions of the uterine horns, body of the uterus and the vagina of adult *Nr5a1*$^{SC-/-}$ mutants. A similar outcome is described in mice lacking MDM2 in SC from E14.5 (Fouchécourt et al., 2016).

In addition, *Nr5a1*$^{SC-/-}$ mutants display normal Wolffian duct-derived genitalia (epididymis, vas deferens, seminal vesicles) (Zhao et al., 2019). These develop under the influence of testosterone, the synthesis of which starts as early as E13.5 in mice (Livera et al., 2006). Their presence indicates therefore that *Nr5a1*$^{SC-/-}$ mutants are exposed to testosterone during fetal development. This is surprising since SC are progressively lost and, with them, is also lost the ability to convert fetal LC-produced androstenedione into testosterone thanks to expression of *Hsd17b1* and *Hsd17b3* (Shima et al., 2013). Thus, another enzyme necessarily compensates for the loss of *Hsd17b1* and *Hsd17b3*, as considered elsewhere (Rebourcet et al., 2020). In this regard, HSD17B12 is a good candidate since it has been shown to convert androstenedione to testosterone (Blanchard and Luu-The, 2007). If so, a cell-type distinct from fetal LC should be involved because they are not able to produce testosterone from androstenedione (Shima et al., 2013). This production is nevertheless insufficient since AGD and penile bone length, both of which are highly sensitive to testosterone levels between E14.5 and E17.5 in mice (Welsh et al., 2014), are reduced in *Nr5a1*$^{SC-/-}$ mutants.

Differentiation of the other testicular cell-types when SC are lacking NR5A1

Regarding the fate of GC in *Nr5a1*$^{SC-/-}$ testes, the data show that most of them become meiotic and die. This may seem strange given that the expression of the meiotic suppressor genes *Fgf9* and *Fgfr1* (Bowles et al., 2010) is increased in NR5A1-deficient SC (Table S2). However, the fact that *Cyp26b1* expression is completely lost in NR5A1-deficient SC may explain, on its own, why GC enter meiosis. Actually, CYP26B1 is mandatory in SC to prevent

Development • Accepted manuscript

meiotic initiation and to maintain GC in an undifferentiated state (Li et al., 2009). In addition, the expression of the quiescence-inducing gene *Nanos2* (Saba et al., 2014) is reduced in GC (Table S2). Thus, not only meiotic initiation is not properly prevented, but mitotic quiescence of GC may also be inappropriately promoted in *Nr5a1*$^{SC-/-}$ testes.

As for fetal LC, their specification and/or development is dependent on SC, in particular through to DHH- and PDGF-dependent signalling pathways (Yao et al., 2002; Brennan et al., 2003). Our finding that fetal LC are present in *Nr5a1*$^{SC-/-}$ testes, despite reduced expression of *Dhh* and *Pdgfa* in the SC suggests that these pathways are no longer required beyond E13.5 to allow proper emergence or survival of fetal LC. Our findings are consistent with the persistence of LC in mouse models with SC genetically ablated from E14.5 by using the Diphtheria toxin approach (Rebourcet et al., 2014; Wang et al., 2020). Furthermore, the fetal LC of *Nr5a1*$^{SC-/-}$ testes appear to be functional as testicular transabdominal descent occurs, suggesting normal INSL3 production (Nef and Parada, 1999; Verma-Kurvari et al., 2005).

With respect to PTM cells, they require that fetal SC support their differentiation, in particular by producing DHH and ECM (Clarck et al., 2000; Pierucci-Alves et al., 2001). Accordingly, their survival is compromised when SC are ablated at E14.5 (Rebourcet et al., 2014; Wang et al., 2020). Thus, the loss of SC, the changes in the ECM they produce and the decrease in *Dhh* expression in *Nr5a1*$^{SC-/-}$ testes called into question the fate of the PTM cells. As a matter of fact, the expression of hallmark genes such as *Acta2*, *Tagln* and *Tpm1* (Jeanes et al., 2005, Sohni et al., 2019) is reduced in PTM cells of *Nr5a1*$^{SC-/-}$ mutants (Table S2). Correspondingly, ACTA2 expression appeared to be reduced or even lost in PTM cells, notably in those surrounding the seminiferous cords where AMH expression is decreased or lost in the SC (Fig. S14). This suggests that PTM cells may be affected in *Nr5a1*$^{SC-/-}$ testes.

Knowing that PTM and adult LC derive from a single population of *Wnt5a*+ steroidogenic progenitors (Ademi et al., 2022) and that *Wnt5a* expression is reduced in f *Nr5a1*$^{SC-/-}$ mutants (Table S2), it is conceivable that the alteration of PTM cells during fetal development and the absence of adult LC in PND60 testes are linked. Regarding adult LC, it is also worth noting that very few of them, if any, develop in *Pdgfa*$^{-/-}$ mutants (Gnessi et al., 2000). The reduction of *Pdgfa* expression in SC lacking NR5A1 (Table S2) may therefore be related to the absence of adult LC in *Nr5a1*$^{SC-/-}$ mutants. Further investigation is required to address these issues.

Development • Accepted manuscript

Materials and Methods

Mice

Mice were housed in a licensed animal facility (agreement #C6721837). They were on a mixed C57BL/6 (50%)/129/SvPass (50%) genetic background. All experiments were approved by the local ethical committee (Com'Eth, accreditation APAFIS #18323-2018113015272439_v3), and were supervised by N.B.G., M.M. and N.V., who are qualified in compliance with the European Community guidelines for laboratory animal care and use (2010/63/UE). The *Nr5a1* conditional allele (*Nr5a1*$^{tm1.1Ics}$, also called *Nr5a1*$^{L2/L2}$) was established at the Institut Clinique de la Souris (*i*CS, Illkirch, France), in the context of the French National Infrastructure for Mouse Phenogenomics PHENOMIN (http://www.phenomin.fr). Noon of the day of a vaginal plug was taken as 0.5-day embryonic development (E0.5). All fetuses were collected by caesarean section. Adult mice (PND60) were anesthetized by intraperitoneal injection of a lethal anesthetic mixture made of Xylasin (3 mg/ml) and Ketamine (20 mg/ml), and tissues were immediately fixed by intracardiac perfusion of 4% (w/v) paraformaldehyde (PFA) dissolved in phosphate buffered saline (PBS). With the exception of single cell RNA-sequencing experiments (see below), *Plekha5*$^{Tg(AMH-cre)1Flor}$;*Nr5a1*$^{+/+}$;*Gt(ROSA)26Sor*$^{tm1(EYFP)Cos}$ and *Plekha5*$^{Tg(AMH-cre)1Flor}$;*Nr5a1*$^{L2/L2}$;*Gt(ROSA)26Sor*$^{tm1(EYFP)Cos}$ males are referred to as controls and *Nr5a1*$^{SC-/-}$ mutants, respectively. Generation and genotyping of mice is described in Supplementary Information.

Blood sample collection and testosterone measurement

After anesthesia with a lethal dose of Xylasin and Ketamine as described above, the blood of PND60 adult mice was collected into heparinized Microvette tubes (Sarstedt, Nümbrecht, Germany) by intra-cardiac sampling. The tubes were then centrifuged at 5000 g for 5 minutes and the resulting plasma samples were frozen until further use. Testosterone concentrations were determined by ELISA using a commercially available kit AR E-8000 (LDN, Labor Diagnostika Nord, Nordhorn, Germany). Statistical significance was further assessed by using two-tail Student's *t*-tests.

Morphology, histology, immunohistochemistry and *in situ* hybridization

Following collection, E12.5-E15.5 fetuses and tissues were fixed for 16 hours in 4% (w/v) PFA at 4°C or in Bouin's fluid at 20°C. After removal of the fixative, samples were rinsed in PBS and placed in 70% (v/v) ethanol for long-term storage, external morphology evaluation and organ weight measurement. They were next embedded in paraffin and 5 µm-

Development • Accepted manuscript

thick sections were made. For histology, sections were stained with hematoxylin and eosin (H&E).

For lHC, antigens were retrieved for 1 hour at 95°C either in 10 mM sodium citrate buffer at pH 6.0 or in Tris-EDTA at pH 9.0 (10 mM Tris Base, 1 mM EDTA, 0.05% (v/v) Tween 20). Sections were rinsed in PBS, then incubated with appropriate dilutions of the primary antibodies (Table S6) in PBS containing 0.1% (v/v) Tween 20 (PBST) for 16 hours at 4°C in a humidified chamber. After rinsing in PBST (3 times for 3 minutes each), detection of the bound primary antibodies was achieved for 45 minutes at 20°C in a humidified chamber using Cy3-conjugated or Alexa Fluor 488-conjugated antibodies. Nuclei were counterstained with 4',6-diamidino-2-phenyl-indole (DAPI) diluted at 10 µg/ml in the mounting medium (Vectashield; Vector Laboratories, Newark, CA, USA). ImmPRESS® Polymer Detection Kits MP-7500 and MP-7405 were used according to the manufacturer's protocol (Vector Laboratories). Confocal microscopy, light-sheet microscopy and image processing used for vasculature analysis are described in Supplementary Information. The surface area occupied by YFP-positive cells was measured using a macro command designed for Fiji software (Imaging Center of IGBMC). Data were expressed as percentage of YFP-positive surface areas relative to the entire testis section surface areas. At least four samples were analyzed per genotype. Statistical analysis was done by a two-tail Student *t*-test, assuming equal variances after arcsine transformation of the percentages.

For detection *in situ* hybridizations (ISH), a commercially available kit was used, according to the manufacturer's instructions (RNAscope™ 2.5 HD Reagent kit–RED, Advanced Cell Diagnostics, Cat No 322360). Briefly, deparaffinized sections from PFA-fixed E13.5 fetuses were treated with Hydrogen Peroxide for 10 min, washed and boiled at 100°C in 1X Target Retrieval Reagent for 10 min. Next, Protease IV was then applied for 15 min at 40°C on dehydrated sections and then slides were washed in distilled water. The pre-warmed probes (RNAscope Probe-Mm-Wnt4, Cat No 401101 and RNAscope Probe-Mm-Fst, Cat No 454331, Advanced Cell Diagnostics) were applied on the sections for 2 h at 40°C. The slides were washed in 1X Wash Buffer, and were subjected to a series of signal amplification (AMP 1 to AMP8). Hybridization signals were detected using a chromogenic Fast RED-B/Fast RED-A reagent. The presence of *Wnt4* and *Fst* mRNA was identified as red punctate dots. The sections were counterstained for 3 min with 12.5% (v/v) Harris hematoxylin diluted in distilled water.

Development • Accepted manuscript

BrdU incorporation and TUNEL assays

BrdU (Sigma-Aldrich, Saint-Quentin-Fallavier, France) dissolved at 5 mg/ml in PBS was injected intraperitoneally to pregnant females at 50 mg/kg of body weight. Two hours later, fetuses were collected (E13.5-E15.5), fixed and embedded as described above. BrdU incorporation was detected on 5 µm-thick sections by using an anti-BrdU mouse monoclonal antibody (diluted 1:100) and indirect IHC as described above. At least three samples per stage and per genotype were analyzed. Data were expressed as percentages of BrdU-positive cells related to the number of DDX4-positive cells. Statistical analysis was done by a two-tail Student *t*-test, assuming equal variances after arcsine transformation of the percentages.

TUNEL-positive cells were detected on sections from PFA-fixed samples using the In Situ Cell Death Detection Kit, Fluorescein, according to the manufacturer's instructions (Roche, Mannheim, Germany). At least three samples were analyzed per genotype. Data were expressed as the ratio between the number of TUNEL-positive cells quantified on entire sections and the surface areas of the testis sections (μm^2). Statistical significance was assessed by using two tail Student's *t*-tests.

Real-time RT-qPCR analyses of RNA extracted from whole testes

Fetal testes were dissected, isolated from mesonephros, snap frozen in liquid nitrogen and stored at –80°C until use. Whole testis total RNA was extracted using RNeasy Mini Kit (Qiagen, Les Ulis, France). RT-qPCR was performed on 5 ng RNA aliquots using Luna® Universal One-Step RT-qPCR Kit, according to the manufacturer's instructions (New England Biolabs, Evry, France). The primers are listed in Table S7. Triplicates of at least four samples were used for each genotype, at each stage. The relative transcript levels were determined using the ΔΔCt method, and normalized to *Acta* whose expression is not affected by ablation of *Nr5a1*.

Purification of YFP-positive Sertoli cells

To dissociate cells, the testes of controls and mutants were incubated for 10 minutes at 37°C in 350 µl of trypsin/EDTA 0.05% (w/v), phenol red solution (Gibco Invitrogen, Auckland, New-Zealand), filtered through a 70 µm cell strainer to generate single cell suspensions, centrifuged at 3000g and suspended in 300 µl PBS as described (Stévant et al., 2018). The YFP-positive and -negative cells were sorted separately by FACS using an Aria® II flow cytometer (BD Biosciences, Le Pont de Claix, France). Sorted cell suspensions were then

Development • Accepted manuscript

lysed for overnight at 55°C in a proteinase K-containing buffer, DNA was extracted and genotyped by PCR using standard protocols and primers as indicated above.

Cell preparation of single cell RNA sequencing

Testes from E13.5 and E14.5 *Nr5a1*$^{L2/L2}$ (control) and *Plekha5*$^{Tg(AMH-cre)1Flor}$;*Nr5a1*$^{L2/L2}$; *Gt(ROSA)26Sor*$^{tm1(EYFP)Cos}$ (mutant) fetuses were dissected out in PBS and cell suspensions were prepared as described above. Cell number and viability were determined by a Trypan Blue exclusion assay on a Neubauer Chamber. Samples consisting of > 90% viable cells were processed on the Chromium Controller from 10X Genomics (Leiden, The Netherlands). Ten thousand cells were loaded per well to yield approximately 5000 to 6000 captured cells into nanoliter-scale Gel Beads-in-Emulsion (GEMs). Details about library preparation, sequencing and data processing are described in Supplementary Information.

Analysis of anoikis and measurement of ATP concentration

A total of 914 anoikis-related genes was acquired from GeneCards (https://www.genecards.org), and 88 of these protein coding genes were selected based on a score > 2.0. The overlap of DEGs in *Nr5a1*-deficient SC and anoikis-related genes was visualized using the R package “VennDiagram”. The caspase activity was determined at E13.5 on 8 (control) and 6 (NR5A1-deficient) batches of about 5,000 FACS-purified SC each, using the Caspase-Glo 3/7 assay (Promega, USA). The ability of MSC-1 SC to die from anoikis when their attachment is impaired was tested using the anoikis assay kit ab284938 (Abcam, UK). Briefly, cells were seeded at 30,000 cells/well on normal (uncoated) and anchorage-resistant (hydrogel-coated) plates and incubated for 24 hours. Live cells were detected with the tetrazolium dye MTT (3-(4,5-dimethylthiazol-2-yl)-2,5-diphenyltetrazolium bromide) assay or by using calcein acetoxymethyl (calcein AM) fluorescence, while dead and dying cells were detected by using the ethidium homodimer (ethD-1) fluorescent dye, according to the manufacturer’s instructions.

Measurement of ATP levels was performed using 6 batches of about 5,000 FACS-purified SC each, isolated from control and *Nr5a1*$^{SC-/-}$ E13.5 testes. The cells were lysed in a lysis buffer [2 mM 1,4-dithiothreitol; 25 mM Tris-phosphate (pH 7.8); 2 mM 1,2-diaminocyclohexane-N,N,N´,N´-tetraacetic acid; 1.25 mg/ml lysozyme; 2.5 mg/ml Bovine serum albumin; 10% (v/v) glycerol; 1% (v/v) Triton® X-100] and ATP was quantified using ATP determination kit (A22066, Invitrogen, USA), according to the manufacturer’s instructions.

Development • Accepted manuscript

Acknowledgements

The *Nr5a1* mouse mutant line was established at the Institut Clinique de la Souris (PHENOMIN *i*CS) in the Genetic Engineering and Model Validation Department with funds from the ANR (see below). We thank Dr Mohamed A ABU EL MAATY, for his help with the TRP53 mutants. We thank Dr Karima HABBAS, Dr Laure ASSELIN, Dr Ekaterina IVANOVA, Dr Angeliki PLATANIA, Oktay CAKIL and Pierre TILLIOLE for their valuable advices and help throughout the completion of this project. We also thank Pr Anne-Marie LEFRANCOIS-MARTINEZ and Dr Juliette GODIN for discussions and advices. We also thank Dr Christelle THIBAULT-CARPENTIER from the Genomeast platform for her input (http://genomeast.igbmc.fr/). Our warmest thanks go to Elvire GUIOT, Yves LUTZ and Bertrand VERNAY (IGBMC imaging Center) for their help in imaging testicular vasculature, as well as to Patrick REILLY for his editing of the manuscript. Some of the text and figures in this paper formed part of Sirine SOUALI-CRESPO's PhD thesis in the Department of Functional Genomics and Cancer of IGBMC at Strasbourg University in 2021. This research was funded by Agence Nationale pour la Recherche Grants (see below). A CC-BY-4.0 public copyright license has been applied by the authors to the present document and will be applied to all subsequent versions up to the Author Accepted Manuscript arising from this submission, in accordance with the grant's open access conditions.

Competing Interest Statement

The authors declare no competing interests.

Funding

This work was supported by CNRS, INSERM and UNISTRA. It was also granted from Fondation pour la Recherche Médicale (FRM FDT201904008001), Agence Nationale de la Recherche (ANR-16-CE14-0017 ; ARESSERC project), and in part by the grant ANR-10-LABX-0030-INRT, a French State fund managed by the ANR under the frame Programme Investissements d'Avenir labelled ANR-10-IDEX-0002-02.

Data availability

The data sets described in this paper are available at Gene Expression Omnibus (GEO) database under the accession number GSE219271.

Development • Accepted manuscript

References

Ademi, H., Djari, C., Mayère, C., Neirijnck, Y., Sararols, P., Rands, C.M., Stévant, I., Conne, B. and Nef, S. (2022). Deciphering the origins and fates of steroidogenic lineages in the mouse testis. *Cell Rep.* **39**, 110935. doi:10.1016/j.celrep.2022.110935

Anamthathmakula, P., Miryala, C.S.J., Moreci, R.S., Kyathanahalli, C., Hassan, S.S., Condon, J.C. and Jeyasuria, P. (2019). Steroidogenic Factor 1 (Nr5a1) is Required for Sertoli Cell Survival Post Sex Determination. *Sci. Rep.* **9**, 4452. doi:10.1038/s41598-019-41051-1

Arango, N.A., Lovell-Badge, R. and Behringer, R.R. (1999). Targeted mutagenesis of the endogenous mouse Mis gene promoter: in vivo definition of genetic pathways of vertebrate sexual development. *Cell* **99**, 409-419. doi:10.1016/s0092-8674(00)81527-5

Baba, T, Otake, H, Sato, T, Miyabayashi, K, Shishido, Y, Wang, CY, Shima, Y, Kimura, H, Yagi, M, Ishihara, Y et al. (2014). Glycolytic genes are targets of the nuclear receptor Ad4BP/SF-1. *Nat. Commun.* **5**, 3634. doi:10.1038/ncomms4634.

Barrionuevo, F., Georg, I., Scherthan, H., Lécureuil, C., Guillou, F., Wegner, M. and Scherer, G. (2009). Testis cord differentiation after the sex determination stage is independent of Sox9 but fails in the combined absence of Sox9 and Sox8. *Dev. Biol.* **327**, 301-312. doi:10.1016/j.ydbio.2008.12.011

Beverdam, A., Svingen, T., Bagheri-Fam, S., McClive, P., Sinclair, A.H., Harley, V.R. and Koopman, P. (2010). Protein tyrosine kinase 2 beta (PTK2B), but not focal adhesion kinase (FAK), is expressed in a sexually dimorphic pattern in developing mouse gonads. *Dev. Dyn.* **239**, 2735-2741. doi:10.1002/dvdy.22396

Bitgood, M.J., Shen, L. and McMahon, A.P. (1996). Sertoli cell signaling by Desert hedgehog regulates the male germline. *Curr. Biol.* **6**, 298-304. doi:10.1016/s0960-9822(02)00480-3

Blanchard, P.G. and Luu-The, V. (2007). Differential androgen and estrogen substrates specificity in the mouse and primates type 12-17beta-hydroxysteroid dehydrogenase. *J. Endocrinol.* **194**, 449-455. doi:10.1677/JOE-07-0144

Bowles, J., Feng, C.W., Spiller, C., Davidson, T.L., Jackson, A. and Koopman, P. (2010). FGF9 suppresses meiosis and promotes male germ cell fate in mice. *Dev. Cell* **19**, 440-449. doi:10.1016/j.devcel.2010.08.010

Development • Accepted manuscript

Brennan, J., Tilmann, C. and Capel, B. (2003). Pdgfr-alpha mediates testis cord organization and fetal Leydig cell development in the XY gonad. *Genes Dev.* **17**, 800-810. doi:10.1101/gad.1052503

Buganim, Y., Itskovich, E., Hu, Y.C., Cheng, A.W., Ganz, K., Sarkar, S., Fu, D., Welstead, G.G., Page D.C. and Jaenisch, R. (2012). Direct reprogramming of fibroblasts into embryonic Sertoli-like cells by defined factors. *Cell Stem Cell* **11**, 373-386. doi:10.1016/j.stem.2012.07.019

Chassot, A.A., Gillot, I. and Chaboissier, M.C. (2014). R-spondin1, WNT4, and the CTNNB1 signaling pathway: strict control over ovarian differentiation. *Reproduction* **148**, R97-R110. doi:10.1530/REP-14-0177

Chen, S.R., Chen, M., Wang, X.N., Zhang, J., Wen, Q., Ji, S.Y., Zheng, Q.S., Gao, F. and Liu, Y.X. (2013). The Wilms tumor gene, Wt1, maintains testicular cord integrity by regulating the expression of Col4a1 and Col4a2. *Biol. Reprod.* **88**, 56. doi:10.1095/biolreprod.112.105379

Clark, A.M., Garland, K.K. and Russell, L.D. (2000). Desert hedgehog (Dhh) gene is required in the mouse testis for formation of adult-type Leydig cells and normal development of peritubular cells and seminiferous tubules. *Biol. Reprod.* **63**, 1825-1838. doi:10.1095/biolreprod63.6.1825

Cool, J., DeFalco, T. and Capel, B. (2012). Testis formation in the fetal mouse: dynamic and complex de novo tubulogenesis. *Wiley Interdiscip. Rev. Dev. Biol.* **1**, 847-859. doi:10.1002/wdev.62

De Santa Barbara, P., Bonneaud, N., Boizet, B., Desclozeaux, M., Moniot, B., Sudbeck, P., Scherer, G., Poulat F. and Berta, P. (1998). Direct interaction of SRY-related protein SOX9 and steroidogenic factor 1 regulates transcription of the human anti-Müllerian hormone gene. *Mol. Cell. Biol.* **18**, 6653-6665. doi:10.1128/MCB.18.11.6653

Eggers, S., Ohnesorg, T. and Sinclair, A. (2014). Genetic regulation of mammalian gonad development. *Nat. Rev. Endocrinol.* **10**, 673-683. doi:10.1038/nrendo.2014.163

Fabbri-Scallet, H., de Sousa, L.M., Maciel-Guerra, A.T., Guerra-Júnior, G. and de Mello, M.P. (2020). Mutation update for the NR5A1 gene involved in DSD and infertility. *Hum. Mutat.* **41**, 58-68. doi:10.1002/humu.23916

Fouchécourt, S., Livera, G., Messiaen, S., Fumel, B., Parent, A.S., Marine, J.C. and Monget, P. (2016). Apoptosis of Sertoli cells after conditional ablation of murine double minute 2 (Mdm2) gene is p53-dependent and results in male sterility. *Cell Death Differ.* **23**, 521-530. doi:10.1038/cdd.2015.120

Development • Accepted manuscript

Fröjdman, K. and Pelliniemi, L.J. (1994). Differential distribution of the alpha 6 subunit of integrins in the development and sexual differentiation of the mouse testis. *Differentiation* **57**, 21-29. doi:10.1046/j.1432-0436.1994.5710021.x

Georg, I., Barrionuevo, F., Wiech, T. and Scherer, G. (2012). Sox9 and Sox8 are required for basal lamina integrity of testis cords and for suppression of FOXL2 during embryonic testis development in mice. *Biol. Reprod.* **87**, 99. doi:10.1095/biolreprod.112.101907

Gilmore, A.P. (2005). Anoikis. *Cell Death Differ.* **12 Suppl. 2**, 1473-1477. doi:10.1038/sj.cdd.4401723

Gnessi, L., Basciani, S., Mariani, S., Arizzi, M., Spera, G., Wang, C., Bondjers, C., Karlsson, L. and Betsholtz, C. (2000). Leydig cell loss and spermatogenic arrest in platelet-derived growth factor (PDGF)-A-deficient mice. *J. Cell Biol.* **149**, 1019-1026. doi:10.1083/jcb.149.5.1019

Griswold, M.D. (2018). 50 years of spermatogenesis: Sertoli cells and their interactions with germ cells. *Biol. Reprod.* **99**, 87-100. doi:10.1093/biolre/ioy027

Ikeda, Y., Tagami, A., Maekawa, M. and Nagai, A. (2021). The conditional deletion of steroidogenic factor 1 (Nr5a1) in Sox9-Cre mice compromises testis differentiation. *Sci. Rep.* **11**, 4486. doi:10.1038/s41598-021-84095-y

Jeanes, A., Wilhelm, D., Wilson, M.J., Bowles, J., McClive, P.J., Sinclair, A.H. and Koopman, P. (2005). Evaluation of candidate markers for the peritubular myoid cell lineage in the developing mouse testis. *Reproduction* **130**, 509-516. doi:10.1530/rep.1.00718

Jiménez R., Burgos M. and Barrionuevo F.J. (2021). Sex Maintenance in Mammals. *Genes* (Basel) **12**, 999. doi:10.3390/genes12070999

Jonkers J., Meuwissen, R., van der Gulden, H., Peterse, H., van der Valk, M. and Berns, A. (2001). Synergistic tumor suppressor activity of BRCA2 and p53 in a conditional mouse model for breast cancer. *Nat. Genet.* **29**, 418-425. doi:10.1038/ng747

Josso, N. and Picard, J.Y. (2022). Genetics of anti-Müllerian hormone and its signaling pathway. *Best Pract. Res. Clin. Endocrinol. Metab.* **36**, 101634. doi:10.1016/j.beem.2022.101634

Kashimada, K., Svingen, T., Feng, C.W., Pelosi, E., Bagheri-Fam, S., Harley, V.R., Schlessinger, D., Bowles, J. and Koopman, P. (2011). Antagonistic regulation of Cyp26b1 by transcription factors SOX9/SF1 and FOXL2 during gonadal development in mice. *FASEB J.* **25**, 3561-3569. doi:10.1096/fj.11-184333

Development • Accepted manuscript

Lécureuil, C., Fontaine, I., Crepieux, P. and Guillou, F. (2002). Sertoli and granulosa cell-specific Cre recombinase activity in transgenic mice. *Genesis* **33**, 114-118. doi:10.1002/gene.10100

Li, H., MacLean, G., Cameron, D., Clagett-Dame, M. and Petkovich, M. (2009). Cyp26b1 expression in murine Sertoli cells is required to maintain male germ cells in an undifferentiated state during embryogenesis. *PLoS One* **4**, e7501. doi:10.1371/journal.pone.000750

Li, Y., Zheng, M. and Lau, Y.F. (2014). The sex-determining factors SRY and SOX9 regulate similar target genes and promote testis cord formation during testicular differentiation. *Cell Rep.* **8**, 723-733. doi:10.1016/j.celrep.2014.06.055

Lindeman, R.E., Murphy, M.W., Agrimson, K.S., Gewiss, R.L., Bardwell, V.J., Gearhart, M.D. and Zarkower, D. (2021). The conserved sex regulator DMRT1 recruits SOX9 in sexual cell fate reprogramming. *Nucleic Acids Res.* **49**, 6144-6164. doi:10.1093/nar/gkab448

Livera, G., Delbes, G., Pairault, C., Rouiller-Fabre, V. and Habert, R. (2006). Organotypic culture, a powerful model for studying rat and mouse fetal testis development. *Cell Tissue Res.* **324**, 507-521. doi:10.1007/s00441-006-0167-7

Lu, Q. and Rounds, S. (2012). Focal adhesion kinase and endothelial cell apoptosis. *Microvasc. Res.* **83**, 56-63. doi:10.1016/j.mvr.2011.05.003

Luo, X., Ikeda, Y. and Parker, K.L. (1994). A cell-specific nuclear receptor is essential for adrenal and gonadal development and sexual differentiation. *Cell* **77**, 481-490. doi:10.1016/0092-8674(94)90211-9

Malki, S., Nef, S., Notarnicola, C., Thevenet, L., Gasca, S., Méjean, C., Berta, P., Poulat, F. and Boizet-Bonhoure B. (2005). Prostaglandin D2 induces nuclear import of the sex-determining factor SOX9 via its cAMP-PKA phosphorylation. *EMBO J.* **24**, 1798-1809. doi:10.1038/sj.emboj.7600660

Matoba, S., Hiramatsu, R., Kanai-Azuma, M., Tsunekawa, N., Harikae, K., Kawakami, H., Kurohmaru, M. and Kanai, Y. (2008). Establishment of testis-specific SOX9 activation requires high-glucose metabolism in mouse sex differentiation. *Dev. Biol.* **324**, 76-87. doi:10.1016/j.ydbio.2008.09.004

Matson, C.K., Murphy, M.W., Sarver, A.L., Griswold, M.D., Bardwell, V.J. and Zarkower, D. (2011). DMRT1 prevents female reprogramming in the postnatal mammalian testis. *Nature* **476**, 101-104. doi:10.1038/nature10239

Development • Accepted manuscript

Mayère, C., Regard, V., Perea-Gomez, A., Bunce, C., Neirijnck, Y., Djari, C., Bellido-Carreras, N., Sararols, P., Reeves, R., Greenaway, S. et al. (2022). Origin, specification and differentiation of a rare supporting-like lineage in the developing mouse gonad. *Sci. Adv.* **8**, eabm0972. doi:10.1126/sciadv.abm0972

McGill, G., Shimamura, A., Bates, R.C., Savage, R.E. and Fisher, D.E. (1997). Loss of matrix adhesion triggers rapid transformation-selective apoptosis in fibroblasts. *J. Cell Biol.* **138**, 901-911. doi:10.1083/jcb.138.4.90

McGuinness, M.P., Linder, C.C., Morales, C.R., Heckert, L.L., Pikus, J. and Griswold, M.D. (1994). Relationship of a mouse Sertoli cell line (MSC-1) to normal Sertoli cells. *Biol. Reprod.* **51**, 116-124. doi:10.1095/biolreprod51.1.116

Morohashi, K., Baba, T. and Tanaka, M. (2013). Steroid hormones and the development of reproductive organs. *Sex Dev.* **7**, 61-79. doi:10.1159/000342272

Morohashi, K.I., Inoue, M. and Baba, T. (2020). Coordination of Multiple Cellular Processes by NR5A1/Nr5a1. *Endocrinol. Metab. (Seoul)* **35**, 756-764. doi:10.3803/EnM.2020.402

Mullen, R.D. and Behringer, R.R. (2014). Molecular genetics of Müllerian duct formation, regression and differentiation. *Sex. Dev.* **8**, 281-296. doi:10.1159/000364935

Murphy, M.W., Gearhart, M.D., Wheeler, A., Bardwell, V.J. and Zarkower, D. (2022). Genomics of sexual cell fate transdifferentiation in the mouse gonad. *G3* (Bethesda) **12**, jkac267. doi:10.1093/g3journal/jkac267

Nef, S. and Parada, L.F. (1999). Cryptorchidism in mice mutant for Insl3. *Nat. Genet.* **22**, 295-299. doi:10.1038/10364

Nef, S., Stévant, I. and Greenfield, A. (2019). Characterizing the bipotential mammalian gonad. *Curr. Top. Dev. Biol.* **134**, 167-194. doi:10.1016/bs.ctdb.2019.01.002

Pierucci-Alves, F., Clark, A.M. and Russell, L.D. (2001). A developmental study of the Desert hedgehog-null mouse testis. *Biol. Reprod.* **65**, 1392-1402. doi:10.1095/biolreprod65.5.1392

Piprek, R.P., Kolasa, M., Podkowa, D., Kloc, M. and Kubiak, J.Z. (2018). Transcriptional profiling validates involvement of extracellular matrix and proteinases genes in mouse gonad development. *Mech. Dev.* **149**, 9-19. doi:10.1016/j.mod.2017.11.001

Development • Accepted manuscript

Rebourcet, D., Mackay, R., Darbey, A., Curley, M.K., Jørgensen, A., Frederiksen, H., Mitchell, R.T., O'Shaughnessy, P.J., Nef, S. and Smith, L.B. (2020). Ablation of the canonical testosterone production pathway via knockout of the steroidogenic enzyme HSD17B3, reveals a novel mechanism of testicular testosterone production. *FASEB J.* **34**, 10373-10386. doi:10.1096/fj.202000361R

Rebourcet, D., O'Shaughnessy, P.J., Pitetti, J.L., Monteiro, A., O'Hara, L., Milne, L., Tsai, Y.T., Cruickshanks, L., Riethmacher, D., Guillou, F., et al. (2014). Sertoli cells control peritubular myoid cell fate and support adult Leydig cell development in the prepubertal testis. *Development* **141**, 2139-2149. doi:10.1242/dev.107029

Rotgers, E., Jørgensen, A. and Yao, H.H. (2018). At the Crossroads of Fate-Somatic Cell Lineage Specification in the Fetal Gonad. *Endocr. Rev.* **39**, 739-759. doi:10.1210/er.2018-00010

Saba, R., Kato, Y. and Saga, Y. (2014). NANOS2 promotes male germ cell development independent of meiosis suppression. *Dev. Biol.* 385, 32-40. doi:10.1016/j.ydbio.2013.10.018

Sararols, P., Stévant, I., Neirijnck, Y., Rebourcet, D., Darbey, A., Curley, M.K., Kühne, F., Dermitzakis, E., Smith, L.B. and Nef, S. (2021). Specific Transcriptomic Signatures and Dual Regulation of Steroidogenesis Between Fetal and Adult Mouse Leydig Cells. *Front. Cell Dev. Biol.* **9**, 695546. doi:10.3389/fcell.2021.695546

Sekido, R. and Lovell-Badge, R. (2008). Sex determination involves synergistic action of SRY and SF1 on a specific Sox9 enhancer. *Nature* **453**, 930–934. doi:10.1038/nature06944

Shima, Y., Miyabayashi, K., Haraguchi, S., Arakawa, T., Otake, H., Baba, T., Matsuzaki, S., Shishido, Y., Akiyama, H., Tachibana, T., et al. (2013). Contribution of Leydig and Sertoli cells to testosterone production in mouse fetal testes. *Mol. Endocrinol.* **27**, 63-73. doi:10.1210/me.2012-1256

Sohni, A., Tan, K., Song, H.W., Burow, D., de Rooij, D.G., Laurent, L., Hsieh, T.C., Rabah, R., Hammoud, S.S., Vicini, E. et al. (2019). The Neonatal and Adult Human Testis Defined at the Single-Cell Level. *Cell Rep.* **26**, 1501-1517.e4. doi:10.1016/j.celrep.2019.01.045

Srinivas, S., Watanabe, T., Lin, C.S., William, C.M., Tanabe, Y., Jessell, T.M. and Costantini, F. (2001). Cre reporter strains produced by targeted insertion of EYFP and ECFP into the ROSA26 locus. *BMC Dev. Biol.* **1**, 4. doi:10.1186/1471-213x-1-4

Development • Accepted manuscript

Staack, A., Donjacour, A.A., Brody, J., Cunha, G. R. and Carroll, P. (2003). Mouse urogenital development: a practical approach. *Differentiation* **71**, 402-413. doi:10.1046/j.1432-0436.2003.7107004.x

Stévant, I., Kühne, F., Greenfield, A., Chaboissier, M.C., Dermitzakis, E.T. and Nef, S. (2019). Dissecting Cell Lineage Specification and Sex Fate Determination in Gonadal Somatic Cells Using Single-Cell Transcriptomics. *Cell Rep.* **26**, 3272-3283.e3. doi:10.1016/j.celrep.2019.02.069

Stévant, I., Neirijnck, Y., Borel, C., Escoffier, J., Smith, L.B., Antonarakis, S.E., Dermitzakis, E.T. and Nef, S. (2018). Deciphering Cell Lineage Specification during Male Sex Determination with Single-Cell RNA Sequencing. *Cell Rep.* **22**, 1589-1599. doi:10.1016/j.celrep.2018.01.043

Street, K., Risso, D., Fletcher, R.B., Das, D., Ngai, J., Yosef, N., Purdom, E. and Dudoit, S. (2018). Slingshot: cell lineage and pseudotime inference for single-cell transcriptomics. *BMC Genomics* **19**, 477. doi:10.1186/s12864-018-4772-0

Sumi, E., Iehara, N., Akiyama, H., Matsubara, T., Mima, A., Kanamori, H., Fukatsu, A., Salant, D.J., Kita, T., Arai, H. et al. (2007). SRY-related HMG box 9 regulates the expression of Col4a2 through transactivating its enhancer element in mesangial cells. *Am. J. Pathol.* **170**, 1854-1864. doi:10.2353/ajpath.2007.060899

Tedja, R., Fox, A. and Alvero, A.B. (2021). Detection of Anoikis Using Cell Viability Dye and Quantitation of Caspase Activity. *Methods Mol. Biol.* **2255**, 69-76. doi:10.1007/978-1-0716-1162-3_7

Teletin, M., Vernet, N., Yu, J., Klopfenstein, M., Jones, J.W., Féret, B., Kane, M.A., Ghyselinck, N. B. and Mark, M. (2019). Two functionally redundant sources of retinoic acid secure spermatogonia differentiation in the seminiferous epithelium. *Development* **146**, dev170225. doi:10.1242/dev.170225

Tremblay, J.J. and Viger, R.S. (1999). Transcription factor GATA-4 enhances Müllerian inhibiting substance gene transcription through a direct interaction with the nuclear receptor SF-1. *Mol. Endocrinol.* **13**, 1388-1401. doi:10.1210/mend.13.8.0330

Uhlenhaut, N.H., Jakob, S., Anlag, K., Eisenberger, T., Sekido, R., Kress, J., Treier, A.C., Klugmann, C., Klasen, C., Holter, N.I., et al. (2009). Somatic sex reprogramming of adult ovaries to testes by FOXL2 ablation. *Cell* **139**, 1130-1142. doi:10.1016/j.cell.2009.11.021

Vachon, P.H. (2011). Integrin signaling, cell survival, and anoikis: distinctions, differences, and differentiation. *J. Signal Transduct.* **2011**, 738137. doi:10.1155/2011/73813

Development • Accepted manuscript

Verma-Kurvari, S., Nef, S. and Parada, L.F. (2005). Hormonal regulation of male reproductive tract development. *Ann. N. Y. Acad. Sci.* **1061**, 1-8. doi:10.1196/annals.1336.002

Wang, Y.Q., Cheng, J.M., Wen, Q., Tang, J.X., Li, J., Chen, S.R. and Liu, Y.X. (2020). An exploration of the role of Sertoli cells on fetal testis development using cell ablation strategy. *Mol. Reprod. Dev.* **87**, 223-230. doi:10.1002/mrd.23309

Welsh, M., Suzuki, H. and Yamada, G. (2014). The masculinization programming window. *Endocr. Dev.* **27**, 17-27. doi:10.1159/000363609

Wilhelm, D., Hiramatsu, R., Mizusaki, H., Widjaja, L., Combes, A.N., Kanai, Y. and Koopman, P. (2007). SOX9 regulates prostaglandin D synthase gene transcription in vivo to ensure testis development. *J. Biol. Chem.* **282**, 10553-10560. doi:10.1074/jbc.M609578200

Yao, H.H., Ungewitter, E., Franco, H. and Capel, B. (2015). Establishment of fetal Sertoli cells and their role in testis morphogenesis. In *Sertoli Cell Biology. 2nd edition* (ed. M. D. Griswold) pp. 57-79. Cambridge: Academic Press, Inc. https://doi.org/10.1016/B978-0-12-417047-6.00002-8

Yao, H.H., Whoriskey, W. and Capel, B. (2002). Desert Hedgehog/Patched 1 signaling specifies fetal Leydig cell fate in testis organogenesis. *Genes Dev.* **16**, 1433-1440. doi:10.1101/gad.981202

Zhao, F. and Yao, H.H. (2019). A tale of two tracts: history, current advances, and future directions of research on sexual differentiation of reproductive tracts. *Biol. Reprod.* **101**, 602-616. doi:10.1093/biolre/ioz07

Development • Accepted manuscript

Figures

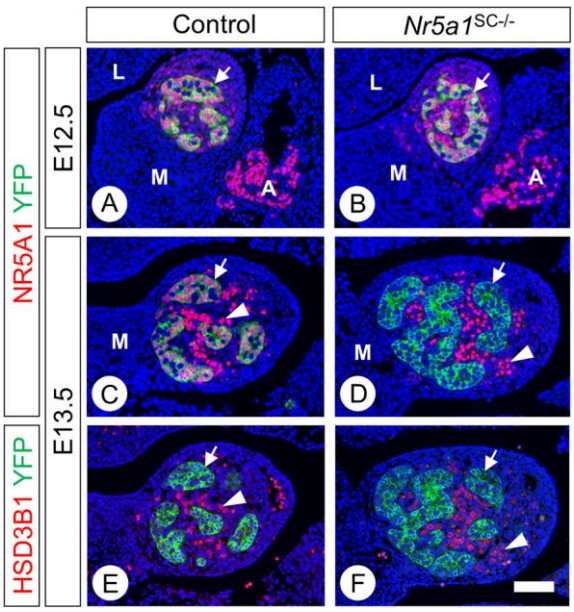

Fig. 1. Ablation of *Nr5a1* in Sertoli cells is efficient from E13.5 onwards. (A-F) Detection of NR5A1 (red nuclear signals), YFP (green cytoplasmic signal), and HSD3B1 (red cytoplasmic signal) by IHC on histological sections of control (A,C,E) and *Nr5a1*$^{SC-/-}$(B,D,F) testes at E12.5 (A,B) and E13.5 (C-F). Efficient excision of the reporter transgene by cre is assessed by YFP expression in SC (arrows) at E12.5 (A,B). However, loss of NR5A1 in SC is only achieved at E13.5 (compare C with D). At this stage, expression of NR5A1 is maintained in Leydig cells (arrowheads in C,D), as identified on consecutive sections by their expression of HSD3B1 (E,F). Nuclei are counterstained with DAPI (blue signal). Scale bar (in F): 50 µm.

Development • Accepted manuscript

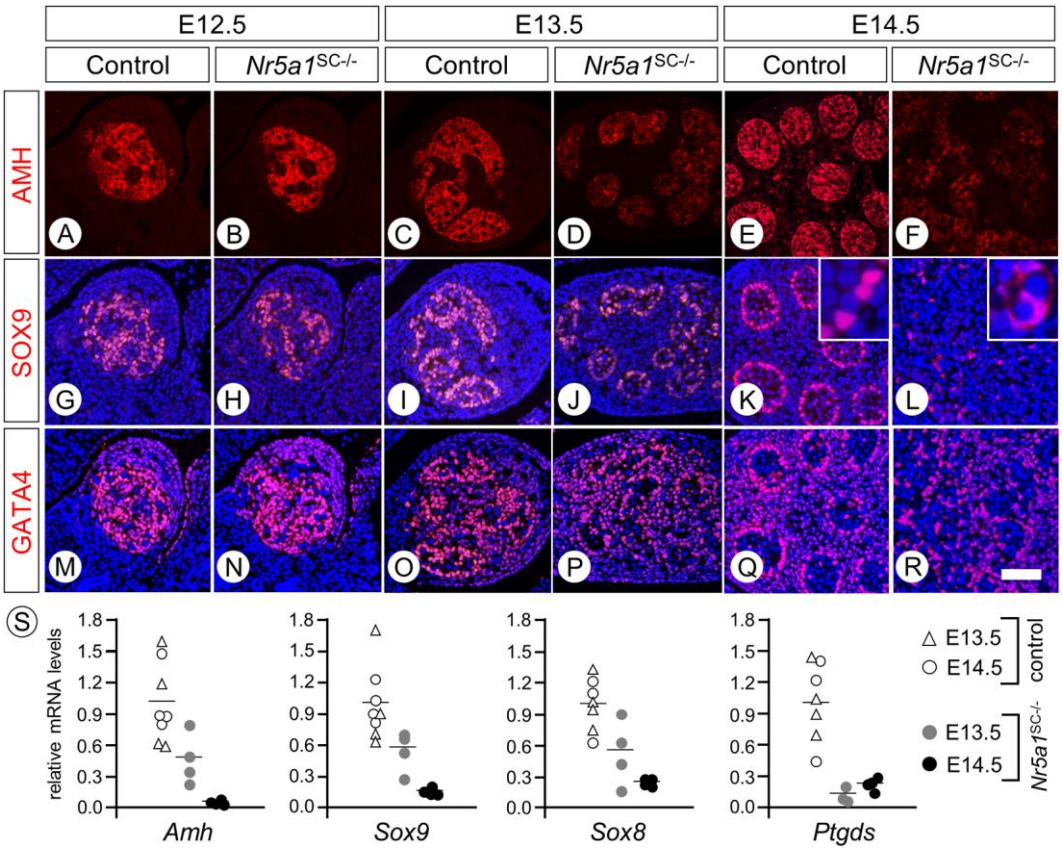

Fig. 2. Ablation of *Nr5a1* in Sertoli cells impairs AMH and SOX9 expression. (A-R) Detection of AMH, SOX9 and GATA4 (red signals) on transverse histological sections of control (A,C,E,G,I,K,M,O,Q) and *Nr5a1*$^{SC-/-}$ (B,D,F,H,J,L,N,P,R) testes at E12.5 (A,B,G,H,M,N), E13.5 (C,D,I,J,O,P) and E14.5 (E,F,K,L,Q,R). Nuclei are counterstained with DAPI (blue signal in G-R). Insets (in K,L) are high magnifications showing nuclear localization of SOX9 in control SC versus cytoplasmic localization in mutant SC. Note that at each developmental stage, detection of AMH, SOX9 and GATA4 was performed on consecutive sections. Scale bar (in R): 50 µm. (S) RT-qPCR analyses comparing the expression levels of *Amh*, *Sox9*, *Sox8* and *Ptgds* mRNAs in whole testis RNA extracted from control (n=4) and *Nr5a1*$^{SC-/-}$ (n=4) testes at E13.5 and E14.5, as indicated. Each point represents the mean value of a technical triplicate, and the bars indicate the mean values.

Development • Accepted manuscript

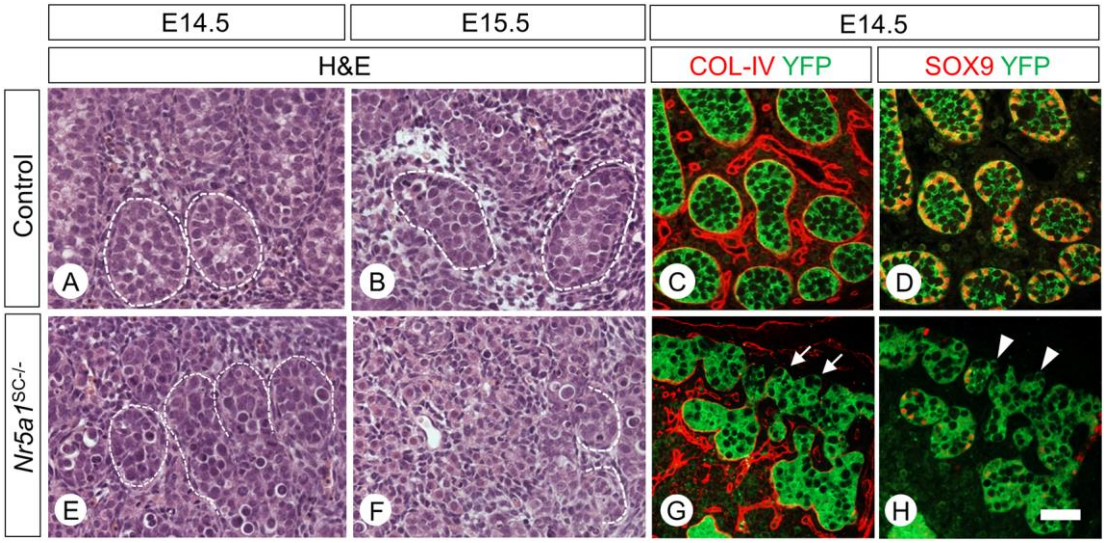

Fig. 3. Ablation of *Nr5a1* in Sertoli cells induces testis cord disorganization. (A,B,E,F) Histological sections through E14.5 (A,E) and E15.5 (B,F) control (A,B) and *Nr5a1*$^{SC-/-}$ (E,F) testes stained by hematoxylin and eosin (H&E). In controls, the seminiferous cords are well defined (closed dotted lines). In mutants, they are poorly defined (open dotted lines). (C,D,G,H) Detection of COL-IV, SOX9 (red signals) and YFP (green signal) on transverse histological sections of control (C,D) and *Nr5a1*$^{SC-/-}$ (G,H) testes at E14.5. Note that (C,D) and (G,H) are consecutive sections. Arrows (in G) point to the loss of COL-IV at the periphery of seminiferous cords, where SOX9 is lost in SC (arrowheads in H). Scale bar (in D): 10 µm (A,B,E,F), 15 µm (C,D,G,H).

Development • Accepted manuscript

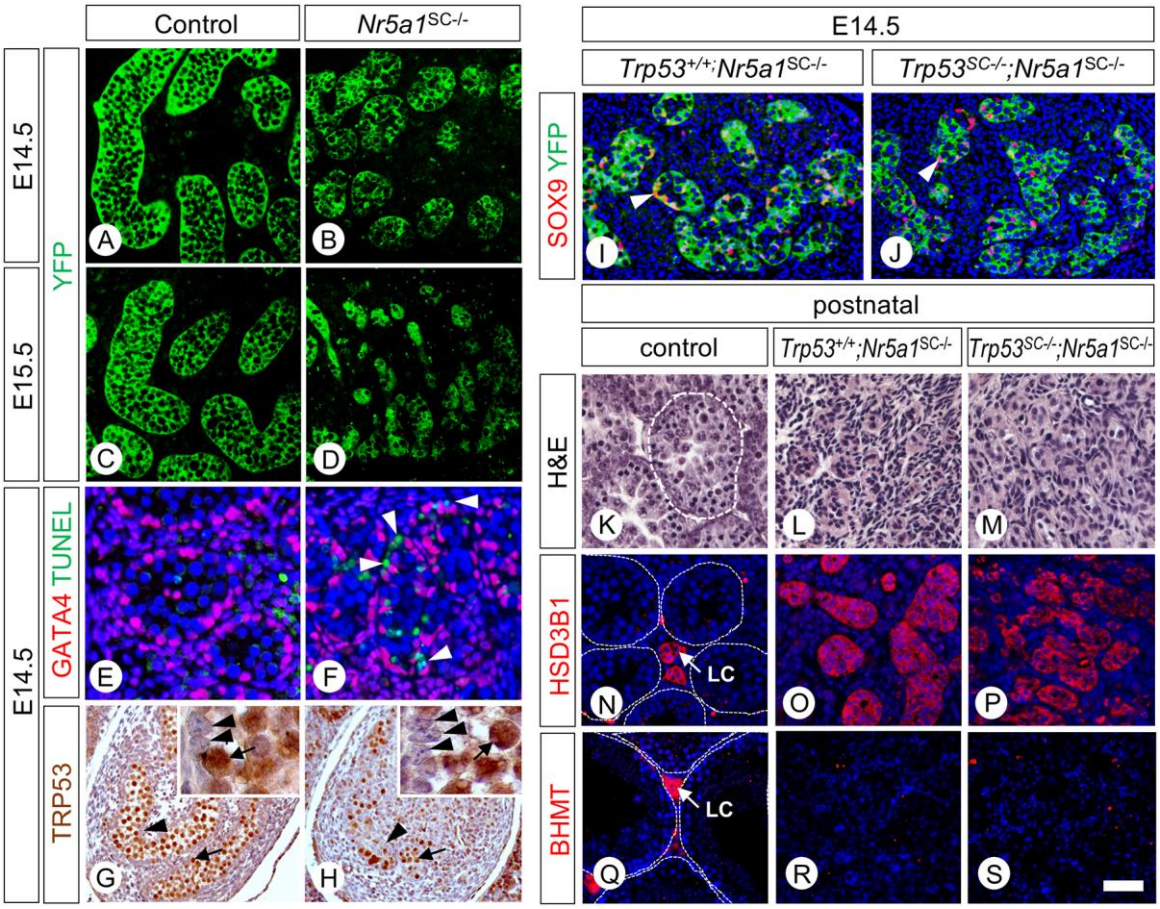

Fig. 4. NR5A1-deficient Sertoli cells die even when they lack TRP53. (A,D) Detection of YFP (green signal) on histological sections from control (A,C) and *Nr5a1*$^{SC-/-}$ (B,D) testes at E14.5 (A,B) and E15.5 (C,D). (E,F) Detection of GATA4 (red signal) and TUNEL-positive cells (green signal) on histological sections of control (E) and *Nr5a1*$^{SC-/-}$ (F) testes at E14.5. Nuclei are counterstained with DAPI (blue signal). Arrowheads point to TUNEL-positive SC in the mutant. (G,H) Detection of TRP53 (brown signal) on histological sections of control (G) and *Nr5a1*$^{SC-/-}$ (H) testes at E14.5. Counterstaining is with H&E. The insets show higher magnifications. Arrowheads and arrows point to SC and GC, respectively. (I,J) Detection of SOX9 (red signal) and YFP (green signal) on histological sections of *Trp53*$^{+/+}$;*Nr5a1*$^{SC-/-}$ (I) and *Trp53*$^{SC-/-}$;*Nr5a1*$^{SC-/-}$ (J) testes at E14.5. Arrowheads point to SC. (K-M) H&E staining of histological sections from control (K), *Trp53*$^{+/+}$;*Nr5a1*$^{SC-/-}$ (L) and *Trp53*$^{SC-/-}$;*Nr5a1*$^{SC-/-}$ (M) testes at PND15. (N-S) Detection of HSB3B1 (N-P) and BHMT (Q-S) (red signals) on histological sections of control (N,Q), *Trp53*$^{+/+}$;*Nr5a1*$^{SC-/-}$ (O,R) and *Trp53*$^{SC-/-}$;*Nr5a1*$^{SC-/-}$ (P,S) testes at PND15 (N-P) and PND60 (Q-S). Nuclei are counterstained with DAPI (blue signal). The dotted white lines (in K,N,Q) delineate seminiferous tubules. LC, Leydig cells. Scale bar (in S): 25 µm (A-D,I,J), 15 µm (E,F), 100 µm (G,H), 80 µm (K-P), 20 µm (Q-S).

Development • Accepted manuscript

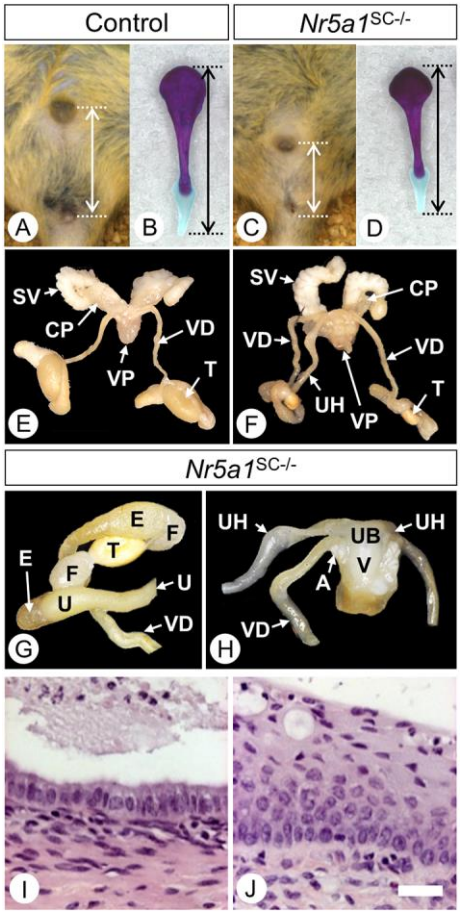

Fig. 5. Abnormal external genitalia and retention of Müllerian duct derivatives in *Nr5a1*$^{SC-/-}$ males. (A,C) Anogenital distance in control (A) and *Nr5a1*$^{SC-/-}$ (B) males at PND60. (B,D) Alizarin red- and alcian blue-stained penis bones from control (A) and *Nr5a1*$^{SC-/-}$ (B) males at PND60. (E-H) Reproductive tracts of control (E) and *Nr5a1*$^{SC-/-}$ (F-H) males at PND60. (I-J) Histological sections through the *Nr5a1*$^{SC-/-}$ genital tract shown in (H) and stained with H&E. The uterine horn displays a simple columnar epithelium (I) and the vaginal epithelium is typically stratified and squamous (J). Legend: A, ampullary gland; CP, cranial prostate; E, epididymis; F, fat pad; SV, seminal vesicle; T, testis; U, uterus, UB, uterus body; UH, uterine horn; V, vagina; VD, vas deferens; VP, ventral prostate. Scale bar (in J): 10 µm (I,J).

Development • Accepted manuscript

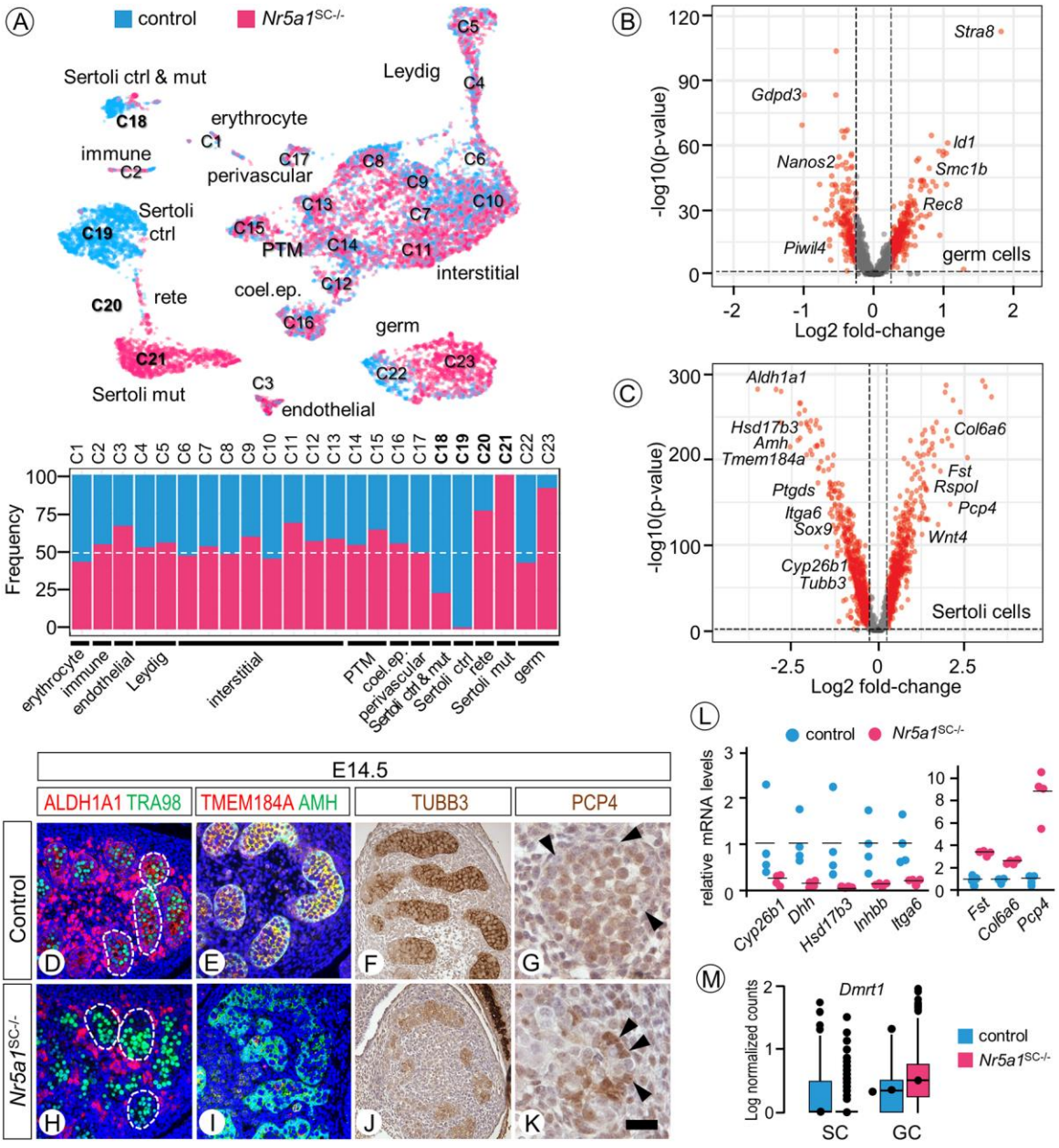

Fig. 6. Transcriptomes of control and *Nr5a1*$^{SC-/-}$ testicular cells at a single-cell resolution. (A) UMAP plot of single cell transcriptomes from control (blue) and *Nr5a1*$^{SC-/-}$ (pink) testes at E14.5, partitioned into 23 cell clusters (named C1-C23) by using Seurat graph-based clustering. The proportion of control and mutant cells in each cluster is indicated below as colored bars. Legend: coel. ep., coelomic epithelium; ctrl, control; mut, mutant. (B,C) Volcano plots of differential gene expression in GC (panel B, clusters C22 and C23) and SC (panel C, clusters C18, C19 and C21) from control and *Nr5a1*$^{SC-/-}$ testes. Red dots correspond to genes dysregulated more than 1.2-fold. (D-K) Detection of ALDH1A1, TMEM184A (red signals), TRA98, AMH (green signals), TUBB3 and PCP4 (brown signals) on transverse histological sections of control (D-G) and *Nr5a1*$^{SC-/-}$ (H-K) testes at E14.5.

Development • Accepted manuscript

Nuclei are counterstained with DAPI (blue signal in D,E,H,I) or with H&E (in F,G,J,K). The dotted lines (in D,H) delimit seminiferous cords. The arrowheads (in G,K) point to SC nuclei. (L) RT-qPCR analyses comparing the expression levels of selected genes using RNA extracted from control (n=4) and *Nr5a1*$^{SC-/-}$ (n=4) whole testes at E14.5. Each point represents the mean value of a technical triplicate, and the bars indicate the mean values. (M) Tukey box plots illustrating medians, ranges and variabilities of log-normalized expression of Dmrt1 in SC and GC, as indicated. Scale bar (in K): 25 µm (D,E,H,I), 100 µm (F,J), 15 µm (G,K).

Development • Accepted manuscript

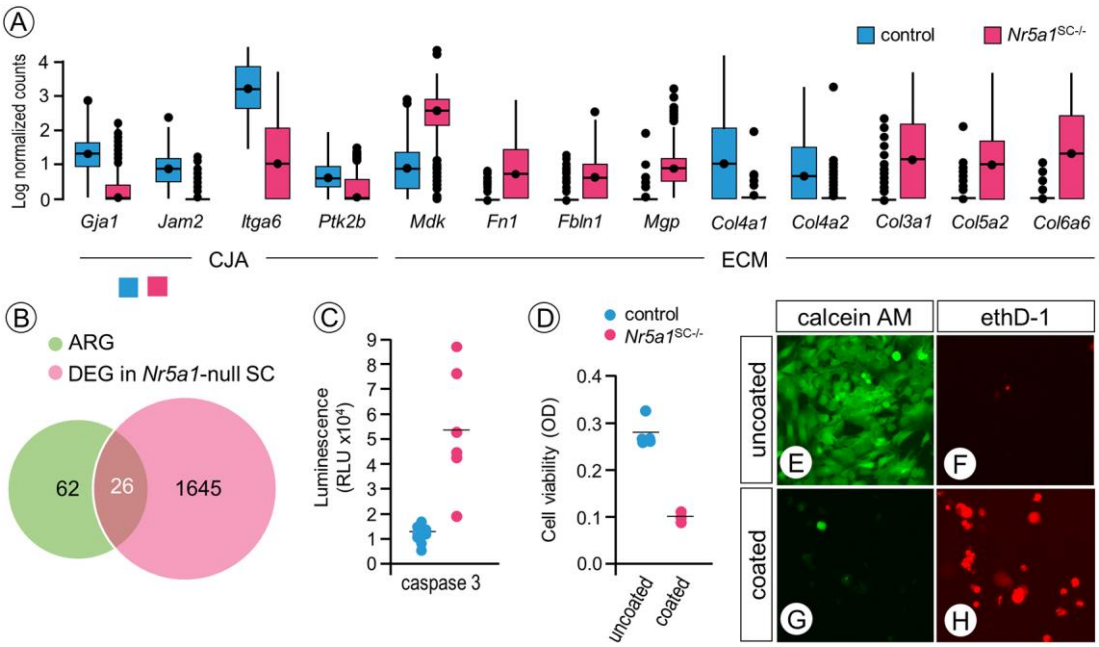

Fig. 7. NR5A1-deficient Sertoli cells die by anoikis. (A) Tukey box plots illustrating medians, ranges and variabilities of log-normalized expression of the selected genes involved in either cell junction/adhesion (CJA) or ECM composition. (B) Venn Diagram showing overlap between anoikis-related genes (ARG) and DEG in NR5A1-deficient SC. (C) Caspase 3 activity measured in FACS-purified control (n=8 batches) and NR5A1-deficient SC (n=6 batches). RLU, relative luminescence units. (D) Cell viability assay using MSC-1 SC plated in control (uncoated, n = 5 wells) or anchorage-resistant (coated, n = 3 wells) plates. Survival of SC is severely compromised when they cannot attach to the plate. Each point (in C,D) represents the value measured for individual batches of SC or individual wells, and the bars indicate the mean values. (E-H) Representative images of anoikis assay using MSC-1 SC seeded on uncoated (E,F) or anchorage-resistant (coated, G,H) plates. Live cells (green signal) were detected with calcein AM (E,F), while dead or dying cells (red signal) were detected with ethD-1 (G,H). The MSC-1 SC can grow in the control (uncoated) plate, but die in the anchorage-resistant (coated) plate.

Development • Accepted manuscript

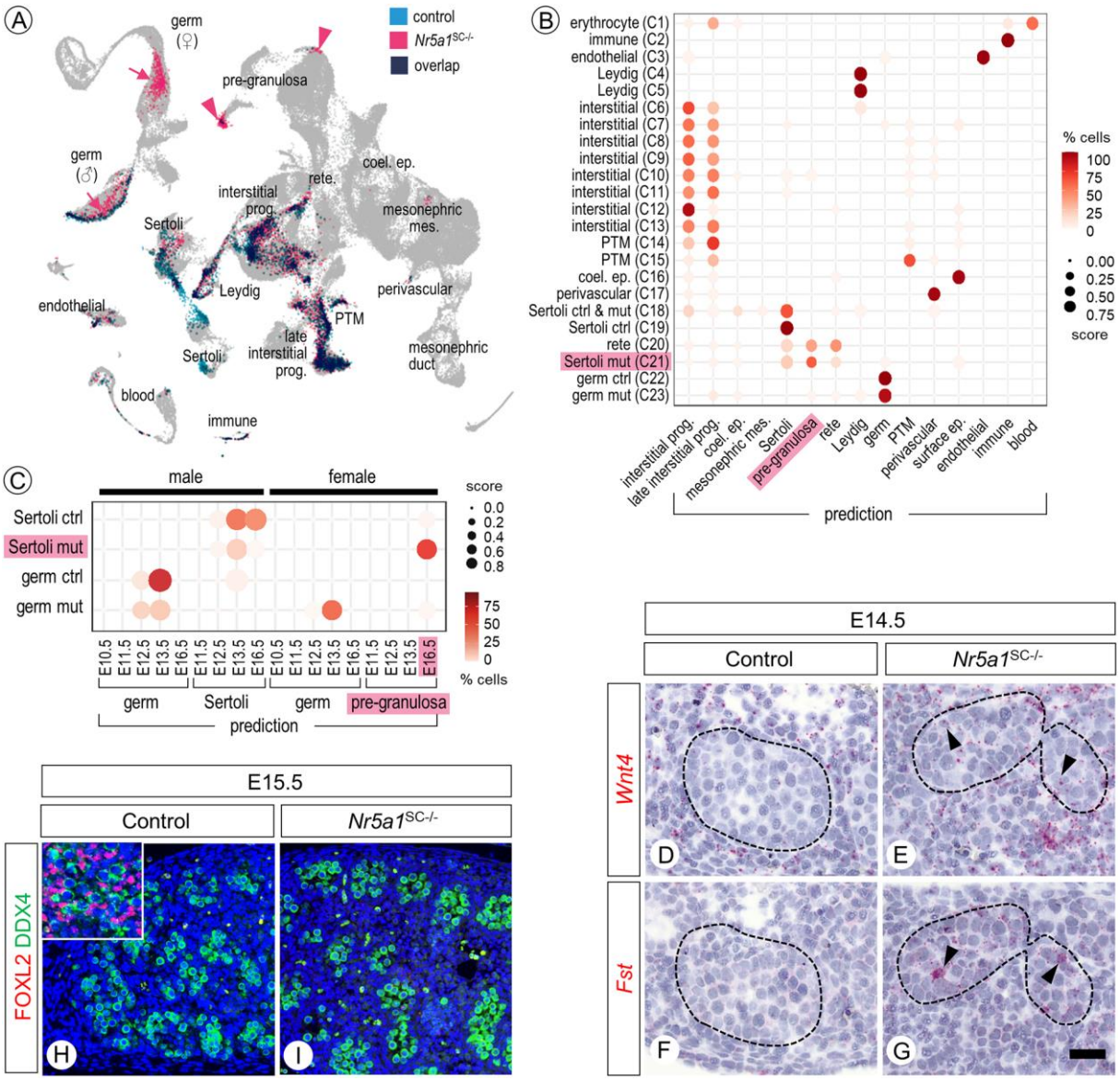

Fig. 8. Ablation of Nr5a1 yields some Sertoli cells to acquire a pre-granulosa-like cell identity. (A) Predicted projection of control (blue) and *Nr5a1*$^{SC-/-}$ (pink) cells on a reference single-cell transcriptomic atlas of gonad development. Arrows and arrowheads point to the locations where GC and SC of the *Nr5a1*$^{SC-/-}$ testes matched best, respectively. (B,C) Dot plots representing the predicted association of cell clusters from the control and *Nr5a1*$^{SC-/-}$ single-cell dataset (y axis) to cell-types (panel B) and to sex and developmental stages (panel C) according to the atlas (x axis). The dot size represents the prediction score (ranging from 0.0 to 1.0) of a given cell cluster to be associated with a given cell-type based on the TransferData function implemented in Seurat. The color intensity (from white to dark red) indicates the percentage of cells of a given cell cluster that have been associated with a given cell-type. Legend: coel. ep., coelomic epithelium; ctrl, control; ep., epithelium; mes., mesenchyme; mut, mutant; prog., progenitor; PTM, peritubular myoid cell. (D-G) *In situ*

Development • Accepted manuscript

hybridization showing expression of *Wnt4* (D,E) and *Fst* (F,G) mRNAs detected by red color staining in control (D,F) and *Nr5a1*$^{SC-/-}$ (E,G) testes at E14.5. Almost no dots were observed in the seminiferous cords of the control testes. In contrast, red dots indicative of *Wnt4* or *Fst* mRNA were present inside the seminiferous cords in *Nr5a1*$^{SC-/-}$testis (arrowheads). The seminiferous cords are delineated by dotted lines. (H,I) Detection of FOXL2 (red signal) and DDX4 (green signal) on transverse histological sections of control (H) and *Nr5a1*$^{SC-/-}$ (I) testes at E15.5. Nuclei are counterstained with DAPI (blue signal). The inset (in H) shows detection of FOXL2 in a E15.5 fetal ovary, used as a positive control for IHC. Scale bar (in G): 15 µm (D-G), 25 µm (H,I).

Development • Accepted manuscript

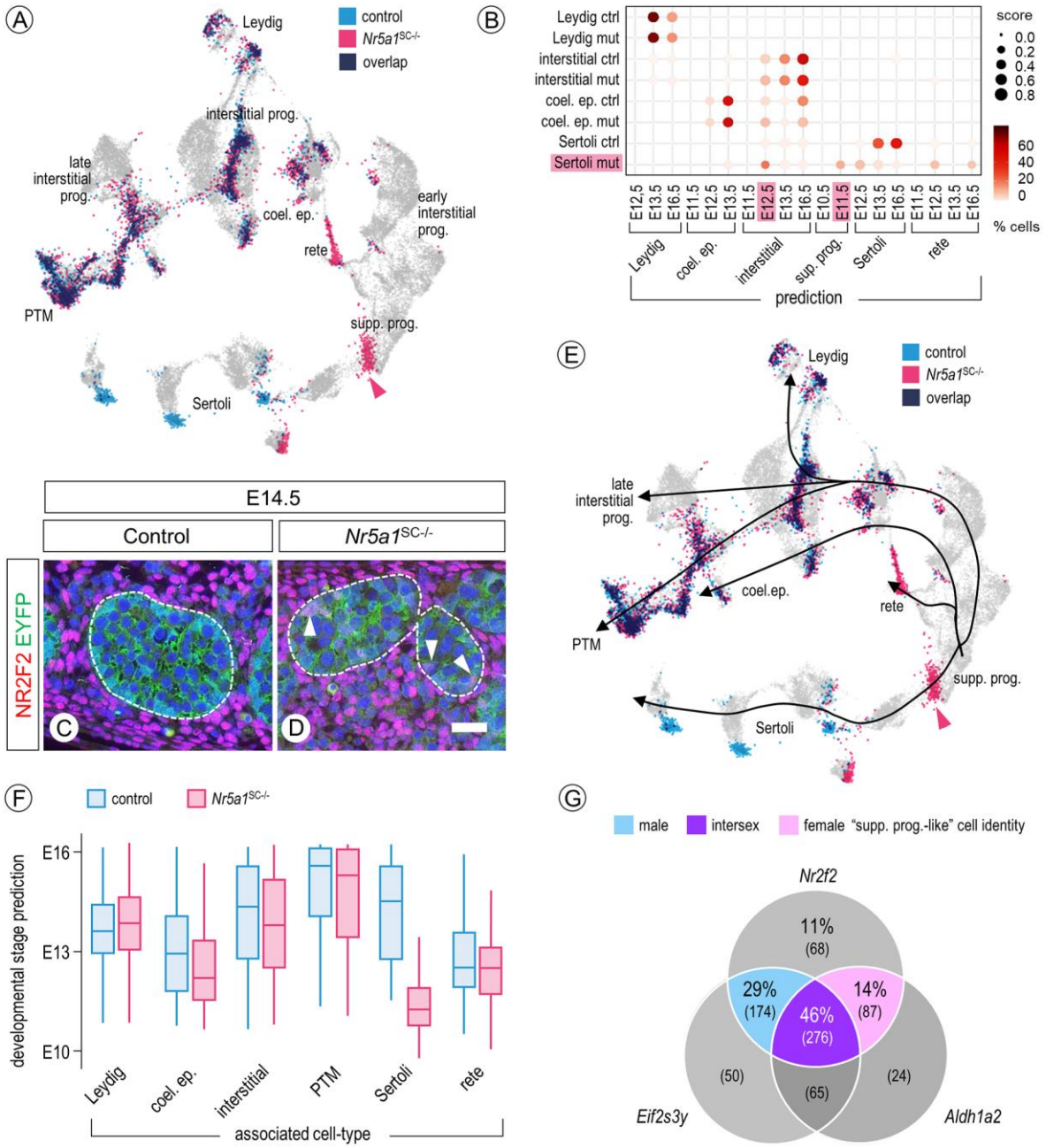

Fig. 9. Ablation of *Nr5a1* yields some Sertoli cells to acquire a "supP-like" cell identity. (A) Predicted projection of control (blue) and *Nr5a1*$^{SC-/-}$ (pink) somatic cells on a reference single-cell transcriptomic atlas of somatic cell development. (B) Dot plots representing the predicted association of cell clusters from the control and *Nr5a1*$^{SC-/-}$ single-cell dataset (y axis) to cell-types and developmental stages according to the atlas (x axis). The dot size represents the prediction score (ranging from 0.0 to 1.0) of a given cell cluster to be associated with a given cell-type based on the TransferData function implemented in Seurat. The color intensity (from white to dark red) indicates the percentage of cells of a given cell cluster that have been associated with a given cell-type. Legend: coel. ep., coelomic

Development • Accepted manuscript

epithelium; ctrl, control; mut, mutant; PTM, peritubular myoid; supp. prog., supporting progenitor. (C,D) Detection of NR2F2 (red signal) and YFP (green signal) on transverse histological sections of control (C) and *Nr5a1*$^{SC-/-}$ (D) testes at E14.5. Nuclei are counterstained with DAPI (blue signal). The arrowheads point to NR5A1-deficient SC (YFP-positive) expressing NR2F2 (pink nuclei). (E) Trajectories inferred over the developmental stages for the major somatic cell-types of the testis superimposed to the predicted projection as in panel A. (F) Boxplot showing the developmental stage prediction for each somatic cell-type of the male control (blue boxes) and *Nr5a1*$^{SC-/-}$ (pink boxes) testes. The population of NR5A1-deficient SC appeared younger (ranging from E10 to E12) than the control SC population (ranging from E12 to E16). (G) Venn diagram showing the percentages of cells expressing *Nr2f2*, *Eif2s3y*, and *Aldh1a2*, alone or in combinations. Cells expressing *Nr2f2* and *Eif2s3y* were assigned a male “supp. prog.-like” cell identity (blue colour), cells expressing *Nr2f2* and *Aldh1a2* were assigned a female “supp. prog.-like” cell identity (pink colour) and cells expressing *Nr2f2*, *Eif2s3y* and *Aldh1a2* were assigned an intersex “supp. prog.-like” identity (purple colour). Scale bar (in D): 15 µm (C,D).

Development • Accepted manuscript

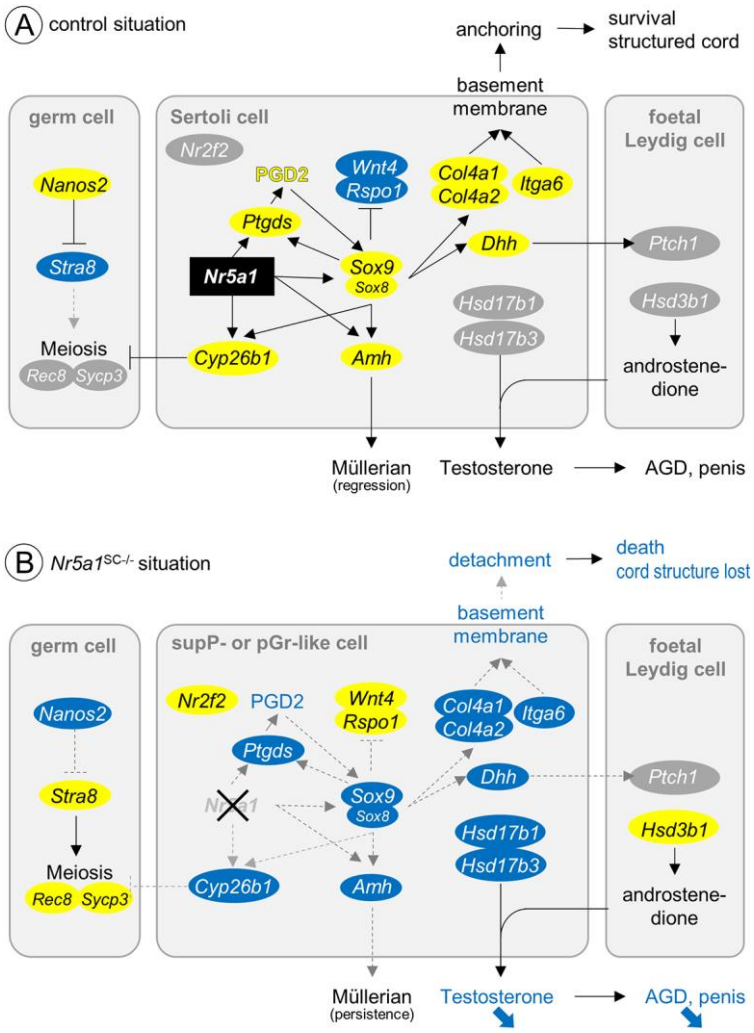

Fig. 10. Summary of the alterations induced by the loss of NR5A1 in Sertoli cells after the sex determination period. (A) Control situation. (B) *Nr5a1*$^{SC-/-}$ situation. Blue and yellow ovals are down - and up -regulated genes, respectively. The decreased expression of *Sox9*, *Amh*, *Cyp26b1* and *Dhh*, in *Nr5a1*$^{SC-/-}$ testes can be ascribed to the loss of NR5A1 in SC since these genes contain NR5A1-binding sites in their regulatory regions (De Santa Barbara et al., 1998; Arango et al., 1999; Sekido and Lovell-Badge, 2008; Kashimada et al., 2011; Li et al., 2014). Legend: AGD, anogenital distance; PGD2, prostaglandin D2; pGr, pre-granulosa; supP, supporting progenitor.

Development • Accepted manuscript

Supplementary Materials and Methods

Mice

To construct the targeting vector a 1.9 kb-long DNA fragment encompassing exon 7 (ENSMUSE00000 693512) was amplified by PCR using 129/SvPass genomic DNA and cloned into an *i*CS proprietary vector containing a *lox*P site, as well as a *lox*P- and *FRT*-flanked neomycin resistance cassette (step1 plasmid). Then, 3 kb- and 3.7 kb-long fragments corresponding to 5' and 3' homology arms were amplified by PCR and introduced into step1 plasmid to generate the targeting construct. This linearized construct was electroporated into 129/SvPass mouse embryonic stem (ES) cells. After selection, targeted clones were identified by PCR using external primers and confirmed by Southern blots (5' and 3' digests) hybridized with neomycin, 5' and 3' external probes. One positive ES clone was injected into C57BL/6J blastocysts. To remove the selection cassette from the *Nr5a1* locus, chimeric males were crossed with *Gt(ROSA)26Sor*$^{tm1(FLP1)Dym}$ females (Farley et al., 2000). Germline transmission was obtained, and a further breeding step was needed to segregate animals bearing the *Nr5a1* L2 allele (also called *Nr5a1*$^{tm1.1Ics}$) from animals bearing the transgene. To inactivate *Nr5a1* in SC, female mice bearing *Plekha5*$^{Tg(AMH\text{-}cre)1Flor}$ (Lécureuil et al., 2002) and *Gt(ROSA)26Sor*$^{tm1(EYFP)Cos}$ (Srinivas et al., 2001) transgenes, and heterozygous for the L2 allele of *Nr5a1* were mated with males heterozygous or homozygous for L2 alleles of *Nr5a1*. The resulting *Plekha5*$^{Tg(AMH\text{-}cre)1Flor}$;*Nr5a1*$^{+/+}$; *Gt(ROSA)26Sor*$^{tm1(EYFP)Cos}$ and *Plekha5*$^{Tg(AMH\text{-}cre)1Flor}$;*Nr5a1*$^{L2/L2}$; *Gt(ROSA)26Sor*$^{tm1(EYFP)Cos}$ males are referred to as control and *Nr5a1*$^{SC\text{-}/\text{-}}$ mutant fetuses, respectively. To test for the role of TRP53, the L2 allele of *Trp53* gene (Jonkers et al., 2001) was further introduced in the mice described above.

Yolk sacs or tail biopsies were taken for DNA extraction. Primers 5'-GTCAAGCGCCCCATGAATGC-3' and 5'-TTAGCCCTCCGATGAGGCTG-3' were first used to amplify *Sry* gene (230 bp-long fragment) for male sex determination. Then, primers 5'-TGAGCCCTGGCACATCCCTCC-3' and 5'-CCTCTGCCCTGCAGGCTTCTG-3' were used to detect *Plekha5*$^{Tg(AMH\text{-}cre)1Flor}$ transgene (273 bp-long amplicon), and primers 5'-AAGGGAGCTG CAGTGGAGTA-3' and 5'-GCCAGAGGCCACTTGTGTAG-3' to detect *Gt(ROSA)26Sor*$^{tm1(EYFP)Cos}$ reporter (520 bp-long amplicon). Primers 5'-CTGTCTCCTGTCTTCTACTACCCTG-3' and 5'-AGCCATTTCAACAGTGCCCCTTCC-3' were used to amplify wild-type (+, 290 bp-long) and

Development • Supplementary information

L2 (400 bp-long) alleles of *Nr5a1*, while primers 5'-GTGGCACATGCATTAGTCCACTTGG-3' and 5'-AGCCA TTTCAACAGTGCCCCTTCC-3' were used to amplify the excised, null, L– (243 bp-long) allele. Primers 5'-CACAAAAACAGGTTAAACCCAG-3' and 5'-AGCACATAGG AGGCAGAGAC-3' were used to amplify the wild-type (288 bp-long) and L2 (370 bp-long) alleles of *Trp53*. Primers 5'-CACAAAAACAGGTTAAACCCAG-3' and 5'-GAAGACAGAAAAG GGGAGGG-3' were used to amplify the excised, null, L– (612 bp-long) allele of *Trp53*. The PCR conditions were 30 cycles with denaturation at 95°C for 30 seconds, annealing at 61°C for 30 seconds and elongation at 72°C for 30 seconds. The amplicons were resolved on 1.5% (w/v) agarose gels, stained by ethidium bromide and visualized under UV light, using standard protocols.

Confocal microscopy, light-sheet microscopy and image analysis

For vasculature imaging, E13.5 embryonic testes were fixed for 4 hours in 4% (w/v) paraformaldehyde, washed in PBS containing 1% (v/v) Triton X-100 and 1% (v/v) dimethyl sulfoxide (DMSO). They were incubated at 4°C for 4 days in PBS containing 0.1% (v/v) Triton X-100 (PBS-X), 1% (v/v) DMSO, 5% (v/v) heat-inactivated normal goat serum, 2% (v/v) heat-inactivated fetal calf serum and the primary antibodies (Table S5). The testes were then washed for 1 day in PBS-X, and incubated for 2 days at 4°C with appropriate Cy3-conjugated or Alexa Fluor 488-conjugated secondary antibodies. They were washed in PBS-X and incubated at room temperature 2 times for 3 hours in clearing solution (Miltenyi Biotec), and 1 hour in ethyl cinnamate. For confocal spinning disk microscopy, cleared testes where mounted onto an Attofluor™ Cell Chamber dish (ThermoFisher Scientific) with a #1.5 cover glass bottom. A Leica 20x/NA 0.75 HC PL APO CS2 objective was used for image acquisition. The following excitation laser lines and detection filter sets were respectively used for the GFP (488 nm, 525-550 nm) and the Cy3 (561 nm, 609-654 nm) labels on a Yokogawa CSU-W1 confocal scanner unit mounted on a Leica DMi8 inverted stand. Stack were acquired with a z-step of 1 µm and 0.322 µm lateral sampling on a Hamamatsu ORCA-Flash4.0 V3 camera. For light sheet microscopy, the testes were embedded in 2% (w/v) low melting point agarose before being cleared. Images were acquired on a Zeiss Lightsheet LS7 equipped with two LSFM 10x/NA 0.2 illumination objectives and an EC Plan-NeoFluar 5x/NA 0.16 detection objective. The excitation lasers line and filters sets were the following for GFP: laser line 488 nm, detection filter 505-545 nm and for Cy3 laser line 561 nm, detection filter 575-615 nm. The calculated light sheet thickness at the waist was 5.67 µm. The stacks were acquired with a z-step of 2.02 µm and 0.54 µm lateral sampling on a Zeiss Axiocam 702 camera. Images where processed in Fiji (Schindelin et al., 2012) for the GFP/Cy3 channels registration and Imaris (Oxford Instruments) for creating the 3D reconstruction of the figures.

Single cell RNA sequencing and data processing

Gel Beads-in-Emulsion (GEMs) were generated by combining barcoded gel beads, a reverse transcription master mix containing cells, and partitioning oil onto Chromium Chip B. Following full length cDNA synthesis and barcoding from poly-adenylated mRNA, GEM were broken and pooled before cDNA amplification by PCR using 11 cycles. After enzymatic fragmentation and size selection, sequencing libraries were constructed by adding Illumina P5 and P7 primers (Illumina, Evry, France), as well as sample index via end repair, A tailing, adaptor ligation and PCR with 10 cycles. Library quantifications and quality controls were determined using Bioanalyzer 2100 (Agilent Technologies, Santa Clara, CA, USA). Libraries were then sequenced on Illumina HiSeq 4000™ as 100 bases paired-end reads, using standard protocols.

Development • Supplementary information

Sequencing data were processed using 10X Genomics software (https://support.10xgenomics.com/). Fastq files were processed with CellRanger (v6.0) on a chimeric genome composed of mm10 *Mus musculus* assembly and 753 bp-long YFP sequence (European Nucleotide Archive accession number AGM20711) (Aliye et al., 2015). The resulting count matrices were aggregated with the Read10X function implemented in Seurat (v4.0.1) (Hao et al., 2021). Cells with less than 200 detected genes and genes detected in less than 10 cells were removed. Doublets were filtered out independently in each individual matrix by using the DoubletFinder R package (v.2.0.2) (McGinnis et al., 2019). Subsequently, the Single-Cell Analysis Toolkit for Gene Expression Data in R (scater v1.10.1) was used to remove outlier cells by using several cell features including the proportions of reads mapping mitochondrial and ribosomal genes, the number of genes and UMIs per cell (McCarthy et al., 2017). Data were normalized using the NormalizeData and the SCT function implemented into Seurat by regressing out the unwanted variation due to cell cycle and to the proportion of mitochondrial genes. The top-3000 most varying genes were used to perform a principal component analysis with the RunPCA function implemented in Seurat. Cells were then clustered by using Seurat graph-based clustering (FindNeighbors and FindClusters functions) on the top-30 principal components, with default parameters. Finally, we used the Uniform Manifold Approximation and Projection (UMAP) method (RunUMAP function) to project cells in a 2D space. Cell clusters were annotated using a set of known marker genes. The FindAllMarkers function implemented in Seurat was used to identify significantly differentially expressed genes (DEGs) between cell clusters. Gene ontology (GO) and pathway enrichment analysis was conducted for each gene expression cluster using the AMEN suite of tools (Chalmel and Primig, 2008) with an BH-adjusted p value of ≤ 0.05. The current dataset was mapped on top of a reference atlas of gonadal development (Mayère et al., 2022) using the FindTransferAnchors and MapQuery functions with default settings. To address this issue, the reference atlas was first processed by using the same pipeline.

For the focused analysis of male gonadal somatic cells, we first selected relevant clusters (i.e. clusters associated with gonadal somatic cell populations such as coelomic epithelial cells, interstitial cells, Leydig cells, rete cells, Sertoli cells, SC) identified from the primary analysis of the current and reference datasets and independently re-analysed the two resulting datasets using the same pipeline. To order male gonadal somatic cells from the reference dataset in pseudotime and infer trajectories over developmental stages, we used the getLineages followed by the getCurves functions using default parameters implemented in the slingshot R package (version 1.8.0) (Street et al., 2018) by indicating the C6 cell cluster (the earliest cluster associated with supporting progeniotor cells) as starting cells and C20 (Leydig cells), C3 (late interstitial cells), C22 (pre-PTM cells), C26 (late epithelial cells), C18 (rete cells) and C15 (SC) as potential ending cells. Numbering of clusters is according to Fig. S11B. As previously described the male gonadal somatic cells from the current dataset were mapped on top of the reference atlas of male gonad somatic cells using the FindTransferAnchors and MapQuery functions with default settings.

Supplementary References

Aliye, N., Fabbretti, A., Lupidi, G., Tsekoa, T. and Spurio, R. (2015). Engineering color variants of green fluorescent protein (GFP) for thermostability, pH-sensitivity, and improved folding kinetics. *Appl. Microbiol. Biotechnol.* **99**, 1205-1216. doi:10.1007/s00253-014-5975-1.

Anamthathmakula, P., Miryala, C.S.J., Moreci, R.S., Kyathanahalli, C., Hassan, S.S., Condon, J.C. and Jeyasuria, P. (2019). Steroidogenic Factor 1 (Nr5a1) is Required for Sertoli Cell Survival Post Sex Determination. *Sci. Rep.* **9**, 4452. doi:10.1038/s41598-019-41051-1

Baba, T, Otake, H, Sato, T, Miyabayashi, K, Shishido, Y, Wang, CY, Shima, Y, Kimura, H, Yagi, M, Ishihara, Y et al. (2014). Glycolytic genes are targets of the nuclear receptor Ad4BP/SF-1. *Nat. Commun.* **5**, 3634. doi:10.1038/ncomms4634.

Best, D., Sahlender, D.A., Walther, N., Peden, A.A. and Adams, I.R. (2008). Sdmg1 is a conserved transmembrane protein associated with germ cell sex determination and germline-soma interactions in mice. *Development* **135**, 1415-1425. doi:10.1242/dev.019497.

Chalmel, F. and Primig, M. (2008). The Annotation, Mapping, Expression and Network (AMEN) suite of tools for molecular systems biology. *BMC Bioinformatics* **9**, 86. doi:10.1186/1471-2105-9-86.

Farley, F.W., Soriano, P., Steffen, L.S. and Dymecki, S.M. (2000). Widespread recombinase expression using FLPeR (flipper) mice. *Genesis* **28**, 106-110. PMID: 11105051

Hao, Y., Hao, S., Andersen-Nissen, E., Mauck, W M.3rd, Zheng, S., Butler, A., Lee, M.J., Wilk, A.J., Darby, C., Zager, M., et al. (2021). Satija, Integrated analysis of multimodal single-cell data. *Cell* **184**, 3573-3587. doi:10.1016/j.cell.2021.04.048.

Ikeda, Y., Tagami, A., Maekawa, M. and Nagai, A. (2021). The conditional deletion of steroidogenic factor 1 (Nr5a1) in Sox9-Cre mice compromises testis differentiation. *Sci. Rep.* **11**, 4486. doi:10.1038/s41598-021-84095-y

Jonkers, J., Meuwissen, R., van der Gulden, H., Peterse, H., van der Valk, M. and Berns, A. (2001). Synergistic tumor suppressor activity of BRCA2 and p53 in a conditional mouse model for breast cancer. *Nat. Genet.* **29**, 418-425. doi:10.1038/ng747.

Lécureuil, C., Fontaine, I., Crepieux, P. and Guillou, F. (2002). Sertoli and granulosa cell-specific Cre recombinase activity in transgenic mice. *Genesis* **33**, 114-118. doi:10.1002/gene.10100.

Mayère, C., Regard, V., Perea-Gomez, A., Bunce, C., Neirijnck, Y., Djari, C., Bellido-Carreras, N., Sararols, P., Reeves, R., Greenaway, S., et al. (2022). Origin, specification and differentiation of a rare supporting-like lineage in the developing mouse gonad. *Sci. Adv.* 8, eabm0972. doi:10.1126/sciadv.abm0972.

McCarthy, D.J., Campbell, K.R., Lun, A.T. and Wills, Q.F. (2017). Scater: pre-processing, quality control, normalization and visualization of single-cell RNA-seq data in R. *Bioinformatics* **33**, 1179-1186. doi:10.1093/bioinformatics/btw77.

McGinnis, C.S., Murrow, L.M. and Gartner, Z.J. (2019). DoubletFinder: Doublet Detection in Single-Cell RNA Sequencing Data Using Artificial Nearest Neighbors. *Cell Syst.* **8**, 329-337. doi:10.1016/j.cels.2019.03.003.

Schindelin, J., Arganda-Carreras, I., Frise, E., Kaynig, V., Longair, M., Pietzsch, T. and Cardona, A. (2012). Fiji: an open-source platform for biological-image analysis. *Nat. Methods* **9**, 676-682. doi:10.1038/nmeth.2019

Development • Supplementary information

Srinivas, S., Watanabe, T., Lin, C.S., William, C.M., Tanabe, Y., Jessell, T.M. and Costantini, F. (2001). Cre reporter strains produced by targeted insertion of EYFP and ECFP into the ROSA26 locus. *BMC Dev. Biol.* **1**, 4. doi:10.1186/1471-213x-1-4.

Street, K., Risso, D., Fletcher, R.B., Das, D., Ngai, J., Yosef, N., Purdom, E. and Dudoit, S. (2018). Slingshot: cell lineage and pseudotime inference for single-cell transcriptomics. *BMC Genomics* **19**, 477. doi:10.1186/s12864-018-4772-0. doi:10.1186/s12864-018-4772-0.

Wang, Y.Q., Cheng, J.M., Wen, Q., Tang, J.X., Li, J., Chen, S.R. and Liu, Y.X. (2020). An exploration of the role of Sertoli cells on fetal testis development using cell ablation strategy. *Mol. Reprod. Dev.* **87**, 223-230. doi:10.1002/mrd.23309

Development • Supplementary information

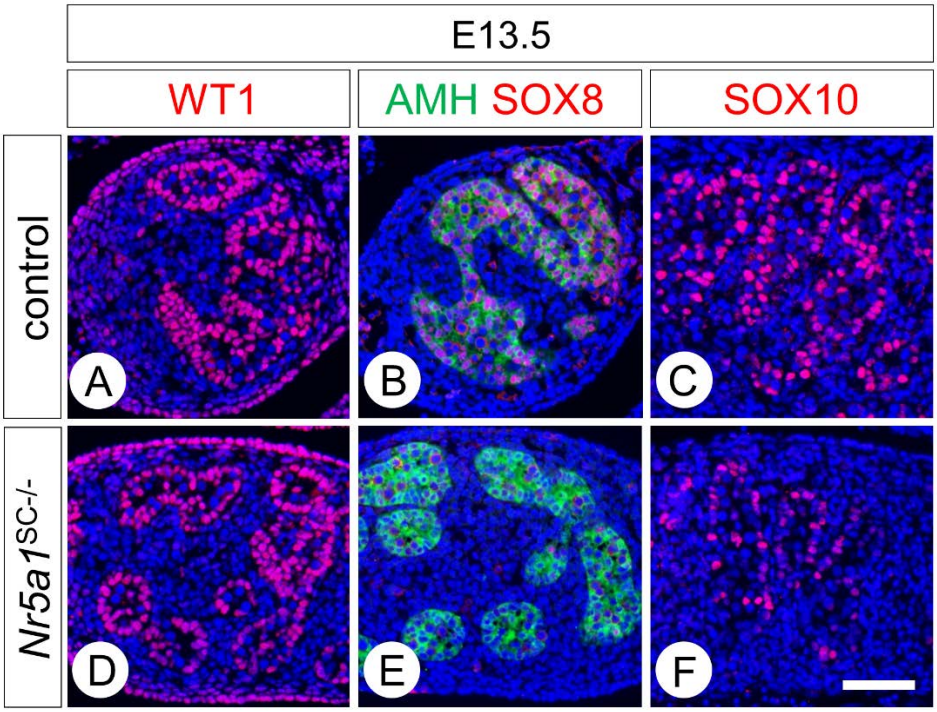

Fig. S1. Ablation of *Nr5a1* in SC impairs SOX8 and SOX10 expression. (A-F) Detection of WT1, SOX8, SOX10 (red signals) and AMH (green signals) on histological sections of control (A-C) and *Nr5a1*$^{SC-/-}$ (D-F) testes at E13.5. Nuclei were counterstained with DAPI (blue signal). Scale bar (in F): 50 µm (A-F).

Development • Supplementary information

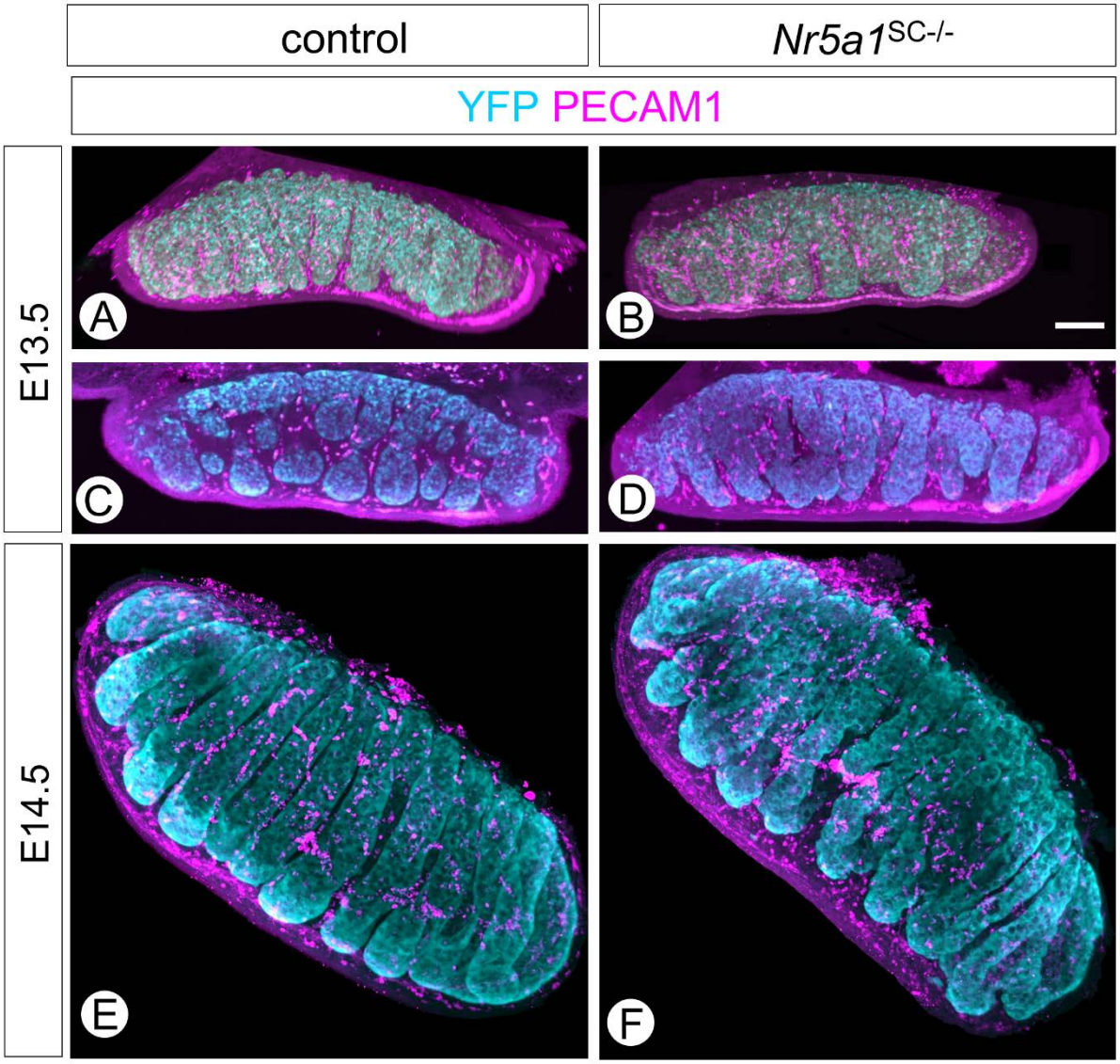

Fig. S2. Ablation of *Nr5a1* in SC does not alter testicular vascularization. (A,B) Detection of YFP in SC (cyan signal) and PCAM1 in vascular cells (magenta signal) using light-sheet microscopy on whole mounts of E13.5 control (A) and *Nr5a1*$^{SC-/-}$ (B) testes. (C,D) Virtual transverse sections made through the testes illustrated in A,B. (E,F) Detection of YFP (cyan signal) and PCAM1 (magenta signal) using confocal spinning disk microscopy on whole mounts of E14.5 control (E) and *Nr5a1*$^{SC-/-}$ (F) testes. The formation of the coelomic artery and of the invading vessels between the seminiferous cords appeared similar between control and *Nr5a1*$^{SC-/-}$testes. Scale bar (in B): 100 µm (A,B), 120 µm (C,D) and 80 µm (E,F).

Development • Supplementary information

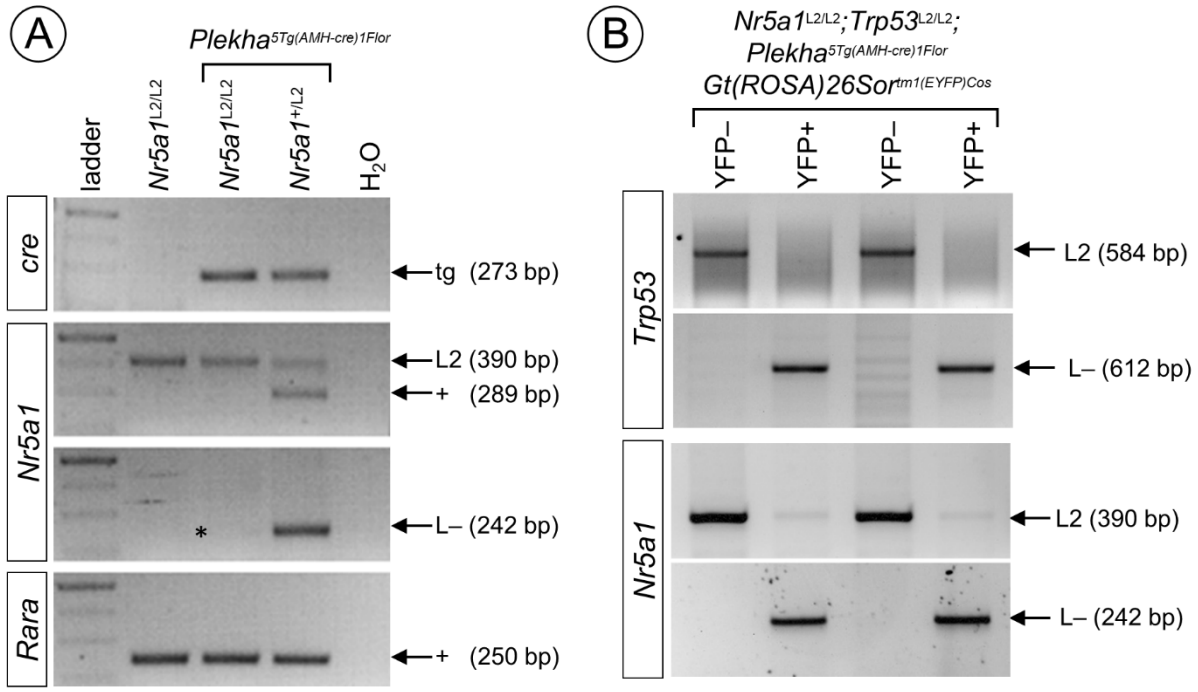

Fig. S3. NR5A1-deficient SC die even in the absence of TRP53. (A) PCR analysis of genomic DNA extracted from control (*Nr5a1*$^{L2/L2}$), mutant (*Plekha5*$^{Tg(AMH\text{-}cre)1Flor}$; *Nr5a1*$^{L2/L2}$) and heterozygote (*Plekha5*$^{Tg(AMH\text{-}cre)1Flor}$; *Nr5a1*$^{+/L2}$) testes of newborns. Upper panel shows genotyping of *Cre* transgene; middle panel shows genotyping of *Nr5a1* alleles; lower panel shows genotyping of *Rara* locus, attesting for an equivalent loading of DNA in each lane. The sizes of the expected fragments are indicated on the right: tg, Cre transgene; L2 and +, *lox*P-flanked and wild-type alleles, L–, excised, null allele. Note that the mutant testis contained only traces of the *Nr5a1* L– allele (asterisk), indicating that SC bearing the excised allele were no longer present at birth. (B) PCR analysis of genomic DNA extracted from FACS-purified YFP-positive (YFP+) and negative (YFP–) cells contained in *Nr5a1*$^{SC–/–}$;*Trp53*$^{SC–/–}$ mutants fetuses at E14.5. Upper panel shows genotyping of *Trp53* alleles; lower panel shows genotyping of *Nr5a1* alleles. The YFP-negative cells (i.e., all cells except SC) contained only the unexcised (L2) alleles, while the YFP-positive cells (i.e., SC) contained only the cre-recombined (L–), null alleles. Note however that traces of the *Nr5a1* L2 alleles were detected in YFP-positive cells.

Development • Supplementary information

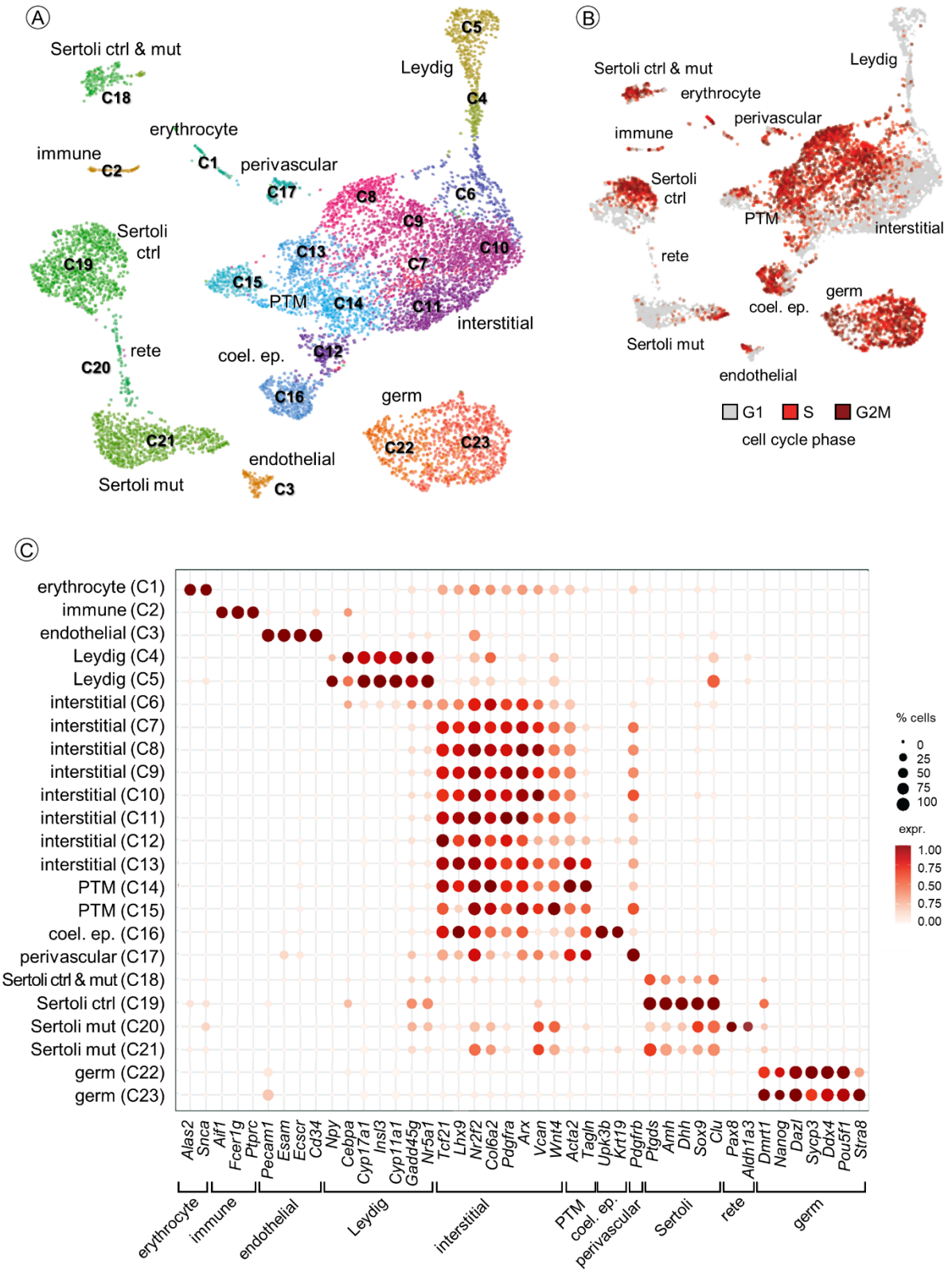

Fig. S4. Identification of cell clusters generated from the single-cell transcriptomes. (A-B) UMAP projection of the 8,998 cells coloured by cell clusters (panel A) or by phases of the cell-cycle, as indicated (panel B). Associated cell annotation is indicated close to the corresponding cell clusters (named C1-23). (C) Dot plot with the expression of selected

Development • Supplementary information

markers (x axis) for each cell cluster (y axis). The dot size represents the percentage of cells expressing a given gene within a given cell cluster. The colour intensity (from light to dark red) indicates the average expression (log normalized counts) of a given gene within a given cell cluster. Legend: coel. ep., coelomic epithelium; ctrl, control; mut, mutant; PTM, peritubular myoid.

Development • Supplementary information

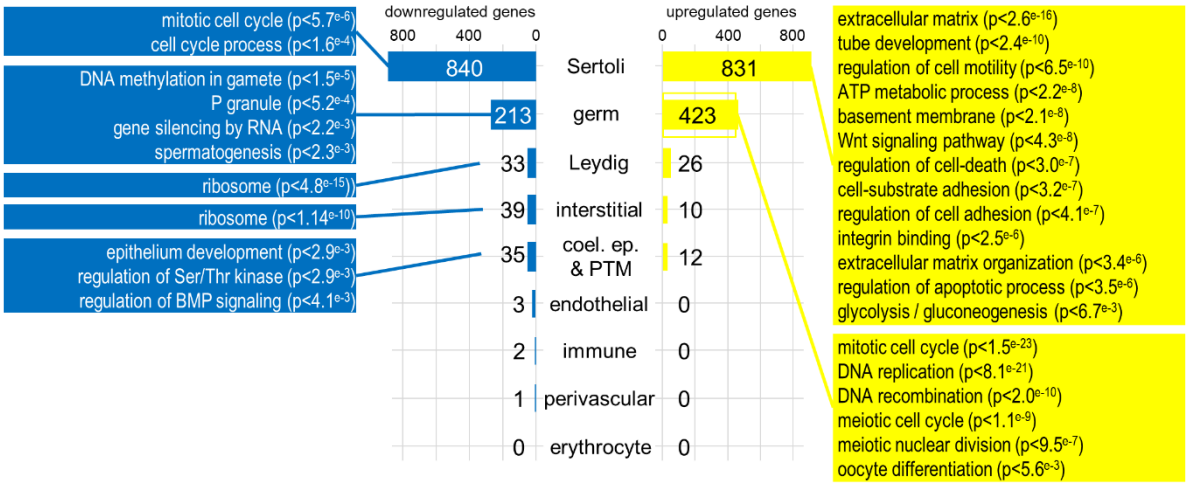

Fig. S5. Number of differentially expressed genes and associated GO terms. Bar plot representing the number of significantly downregulated (left side, in blue) and upregulated (right side, in yellow) genes between control and *Nr5a1*$^{SC-/-}$ cells (x axis), in each cell-type (y axis). Enriched GO terms and their associated *p* values are given for each cell-type. Legend: coel. ep., coelomic epithelium; PTM, peritubular myoid.

Development • Supplementary information

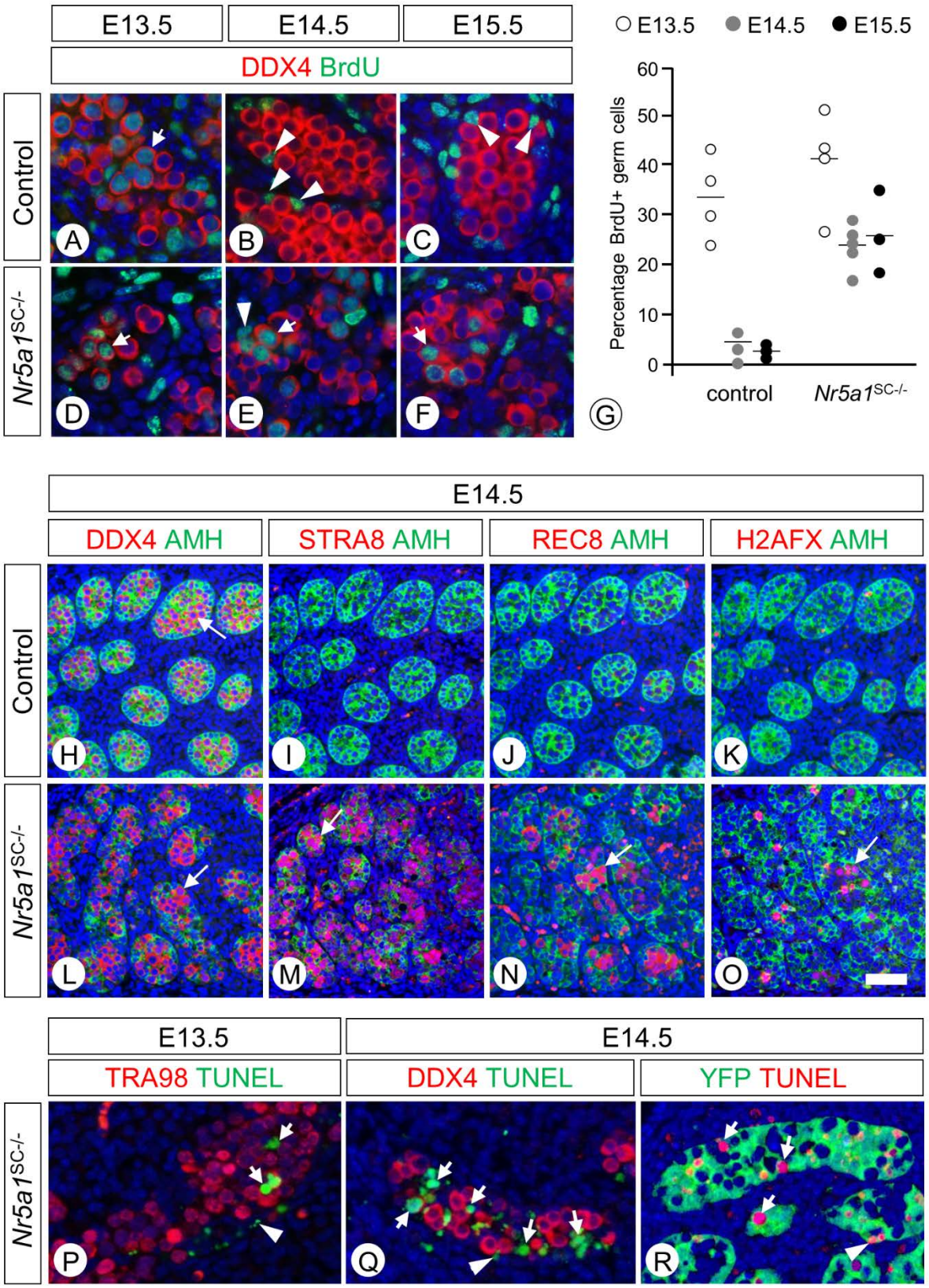

Fig. S6. Germ cells initiate meiosis and die in *Nr5a1*$^{SC-/-}$ mutants. (A-F) Detection of DDX4 (red cytoplasmic signal) and BrdU (green nuclear signal) on histological sections of control (A-C) and *Nr5a1*$^{SC-/-}$ (D-F) testes at E13.5 (A,D), E14.5 (B,E) and E15.5 (C,F). Arrows and arrowheads point to BrdU-positive GC and SC, respectively. (G) Dot plots

Development • Supplementary information

showing the percentage of BrdU-positive GC in control (n=3 to 4) and *Nr5a1*$^{SC-/-}$ (n=3 to 4) testes, as a function of the developmental stages. (H-O) Detection of DDX4, STRA8, REC8, H2AFX (red signals) and AMH (green cytoplasmic signal) on histological sections of control (H-K) and *Nr5a1*$^{SC-/-}$ (L-O) testes at E14.5. Arrows point to GC. The meiotic proteins STRA8, REC8, H2AFX were detected in the mutant but not in the control testes. Arrows point to GC. (P,Q) Detection of TUNEL-positive cells (green signal) and TRA98- or DDX4-positive GC (red signals) on sections from E13.5 (P) and E14.5 (Q) *Nr5a1*$^{SC-/-}$testes. (R) Detection of TUNEL-positive cells (red signal) and YFP-positive SC (green signal) on sections from an E14.5 *Nr5a1*$^{SC-/-}$ testis. Arrows point to TUNEL-positive GC, while arrowheads point to TUNEL-positive SC. The total number of TUNEL-positive cells was significantly larger in *Nr5a1*$^{SC-/-}$ than in control testes [79 ± 9 cell/mm^2 (n=6) versus 27 ± 11 cell/mm^2 (n=3), respectively; $p<0.05$]. Scale bar (in O): 10 µm (A-F,P,R), 50 µm (H-O).

Development • Supplementary information

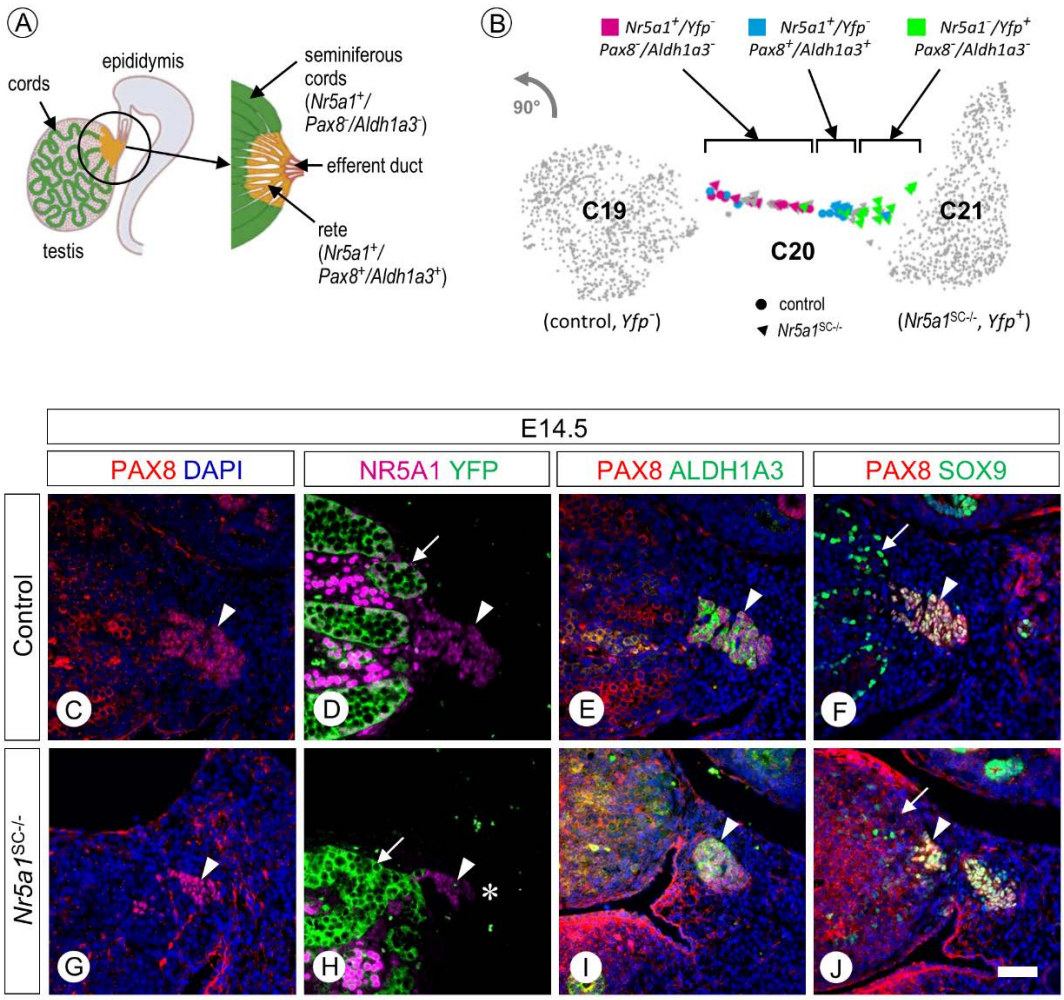

Fig. S7. Cluster C20 corresponds to *rete* testis cells, in which gene excision by cre recombinase is not operational. (A) Diagram illustrating the location and organization of *rete* testis in the mouse. Seminiferous cords are in green, while *rete* testis is in brown. (B) Magnification of UMAP plot (rotated by 90° with respect to Fig. 6) for clusters C19, C20 and C21. Cells belonging to C19 (from control testes, YFP-negative cells) and to C21 (from *Nr5a1*$^{SC-/-}$ testes, YFP-positive) are in grey. Cells belonging to C20 and expressing distinct combination between *Nr5a1*, *Yfp*, *Pax8* and *Aldh1a3* are depicted by a colour code: pink represents cells expressing *Nr5a1* but not *Yfp*, *Pax8* or *Aldh1a3* (SC); blue stands for cells expressing *Nr5a1*, *Pax8* and/or *Aldh1a3*, but not *Yfp* (*rete* testis cells); green represents cells expressing *Yfp* but not *Nr5a1*, *Pax8* or *Aldh1a3* (mutant SC). Circles and triangles represent control and *Nr5a1*$^{SC-/-}$ cells, respectively. Note that the YFP-reporter transgene was absent in the control gonads but present in the *Nr5a1*-deficient gonads used for the scRNA-seq experiments. (C-J) Detection of PAX8 (red signal), NR5A1 (magenta signal) and YFP, ALDH1A3 or SOX9 (green signals) on sections from control (C-F) and *Nr5a1*$^{SC-/-}$ (G-J) testes at E14.5. Note that the YFP-reporter transgene was present in both the control and the *Nr5a1*-deficient gonads used for IHC analysis. Arrows and arrowheads point to SC and *rete* testis cells, respectively. The *rete* testis cells (arrowheads) were PAX8- and ALDH1A3-positive (E,I). They were also NR5A1-positive, YFP-negative and SOX9-positive in both control (D,F) and *Nr5a1*$^{SC-/-}$ testes (H,J). In contrast, SC (arrows) were NR5A1-negative, YFP-positive and SXO9-negative in the *Nr5a1*$^{SC-/-}$ testes (H,J), but NR5A1-positive, YFP-negative and SOX9-positive in the control testes (D,F). Scale bar (in J): 50 µm (C-J).

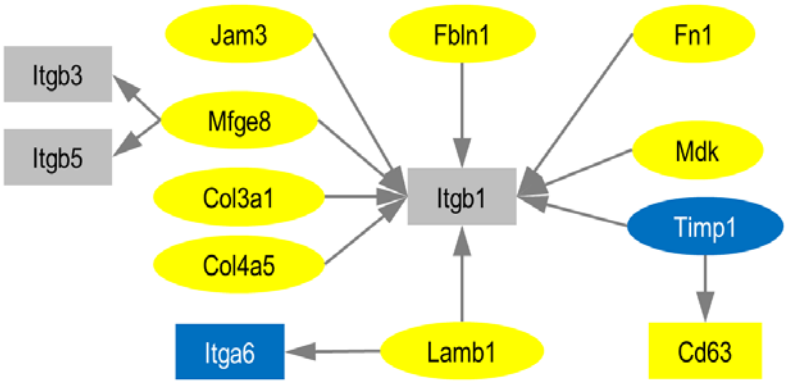

Fig. S8. Selected ligand-receptor interactions between SC and GC. Diagram of the ligand-receptor interactions between SC and GC, as revealed from the single cell transcriptomes. Each node of the network corresponds to a given gene encoding a ligand (oval shape) or a receptor (rectangle shape). Intercellular communication network among SC and GC were predicted using the CellTalkDB database, which contains literature-supported ligand-receptor pairs. Downregulated and upregulated genes are blue and yellow coloured, respectively. Grey boxes indicated receptors whose expression in not changed. The arrows point from the ligand to the receptors.

Development • Supplementary information

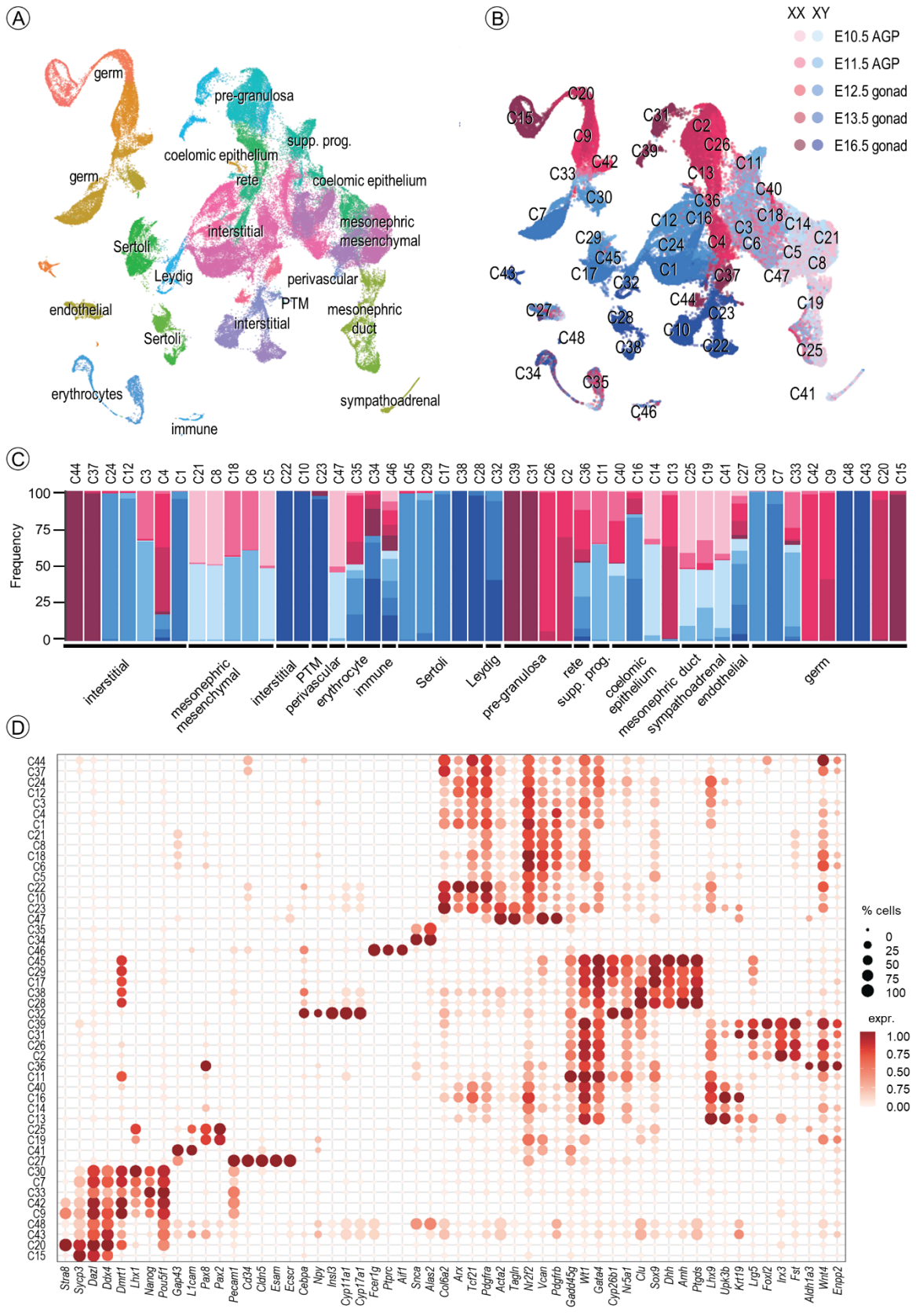

Fig. S9. Identification of cell clusters generated from the atlas. (A-B) UMAP projection of the 94,705 cells from the single-cell transcriptomic atlas of gonad development recently published (Mayère et al., 2022) coloured by cell clusters (in panel A) or by developmental stage, from E10.5 to E16.5 as indicated (in panel B). Cell clusters (C1-C48)

Development • Supplementary information

and their associated cell annotation are indicated. (C) Stacked bar plot showing the proportion of the developmental stages (from light at E10.5 to dark colour at E16.5) amongst the different cell clusters with male (XY, blue) and female (XX, pink) cells. (D) Dot plot with the expression of selected markers (x axis) for each cell cluster (y axis). The dot size represents the percentage of cells expressing a given marker within a given cell cluster. The colour intensity (from light to dark red) indicates the average expression (expr., log normalized counts) of a given marker within a given cell cluster. Legend: AGP, adrenal-gonadal primordium; E, embryonic day; PTM, peritubular myoid cells; supp. prog., supporting progenitor cells; XX, female, XY, male.

Development • Supplementary information

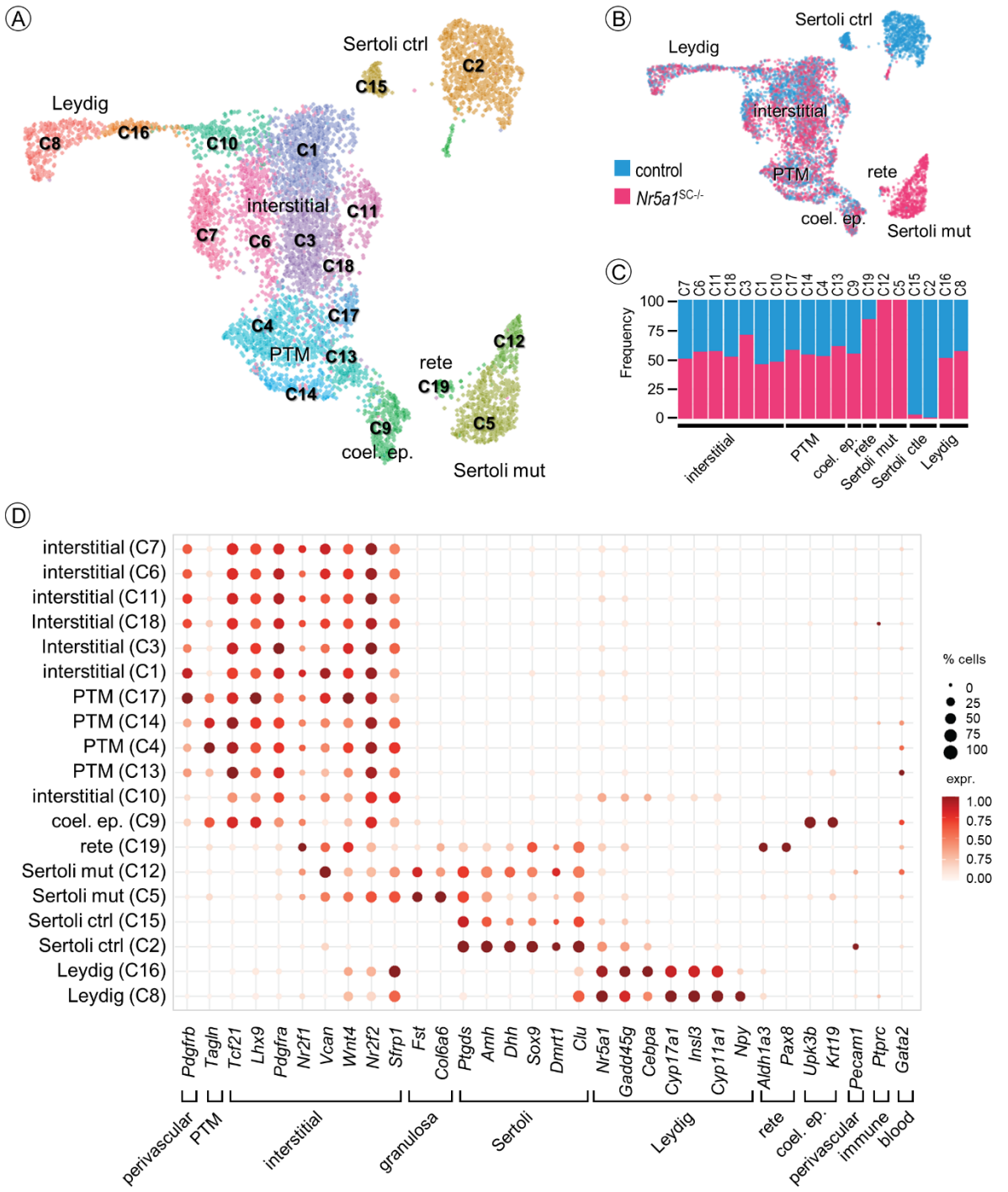

Fig. S10. Identification of cell clusters generated from the single-cell transcriptomes of gonad somatic cells only. (A-B) UMAP projection of the 8,998 cells coloured by cell clusters (panel A) or by genotype, as indicated (panel B). Associated cell annotation is indicated close to the corresponding cell clusters (named C1-C19). (C) Proportions of control and mutant cells in each cluster is indicated as coloured bars. Legend: Legend: coel. ep., coelomic epithelium; ctrl, control; mut, mutant; PTM, peritubular myoid cells. (D) Dot plot with the expression of selected markers (x axis) for each cell cluster (y axis). The dot size represents the percentage of cells expressing a given gene within a given cell cluster. The colour intensity (from light to dark red) indicates the average expression (log normalized counts) of a given gene within a given cell cluster.

Development • Supplementary information

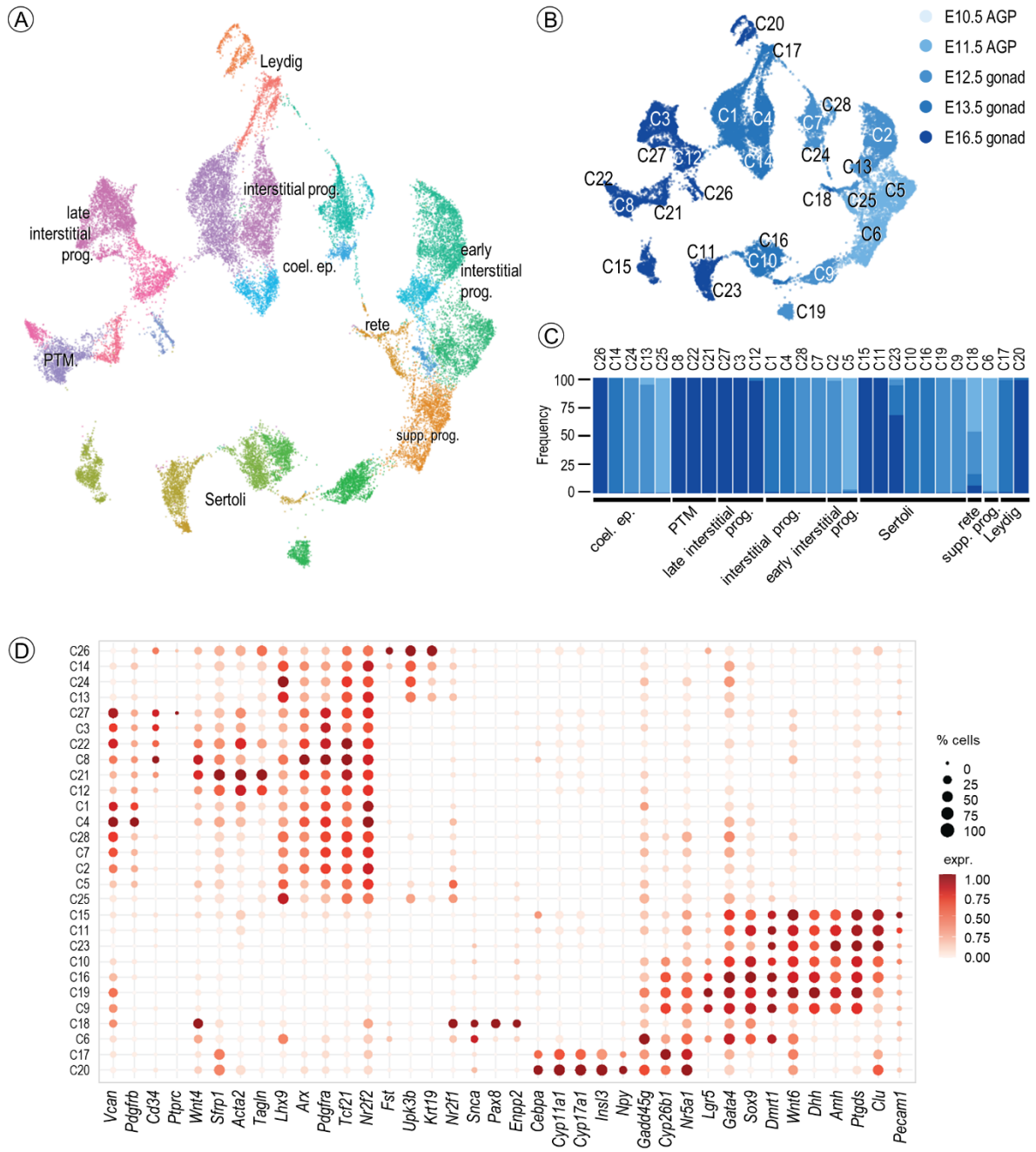

Fig. S11. Identification of somatic male cell clusters generated from the atlas. (A-B) UMAP projection of the male somatic cells from the single-cell transcriptomic atlas of gonad development (Mayère et al., 2022) coloured by cell clusters (in panel A) or by developmental stage, from E10.5 to E16.5 as indicated (in panel B). Cell clusters (C1-C28) and their associated cell annotation are indicated. (C) Stacked bar plot showing the proportion of the developmental stages (from light at E10.5 to dark blue at E16.5) amongst the different male cell clusters. (D) Dot plot with the expression of selected markers (x axis) for each cell cluster (y axis). The dot size represents the percentage of cells expressing a given marker within a given cell cluster. The colour intensity (from light to dark red) indicates the average expression (log normalized counts) of a given marker within a given cell cluster. Legend: AGP, adrenal-gonadal primordium; coel. ep., coelomic epithelium; E, embryonic day; prog., progenitor; PTM, peritubular myoid cells; supp. prog., supporting progenitor cells.

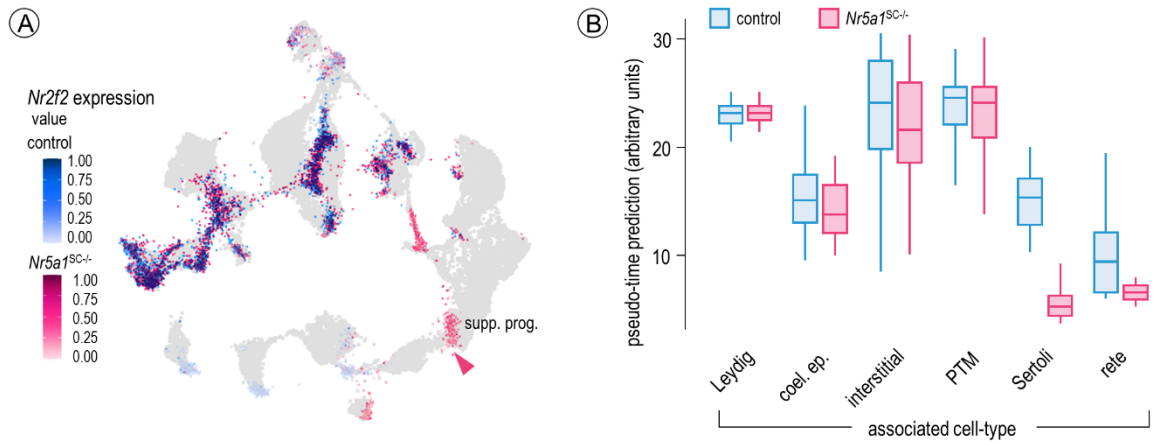

Fig. S12. NR5A1-deficient SC express *Nr2f2* and display a transcriptomic signature corresponding to an earlier stage of development for SC. (A) Expression of *Nr2f2* in control (blue) and *Nr5a1*$^{SC-/-}$ (pink) somatic cells projected on the reference single-cell transcriptomic atlas of male somatic cell development (Mayère et al., 2022). The color intensity (from white to dark blue or dark pink) indicates the level of expression. (B) Boxplot showing the pseudo time prediction for each of the major somatic cell-types of the control (blue boxes) and *Nr5a1*$^{SC-/-}$ (pink boxes) testes. The NR5A1-deficient SC population appears younger than the control SC population. Legend: coel. ep., coelomic epithelium; PTM, peritubular myoid cells; supp. prog., supporting progenitor cells.

Development • Supplementary information

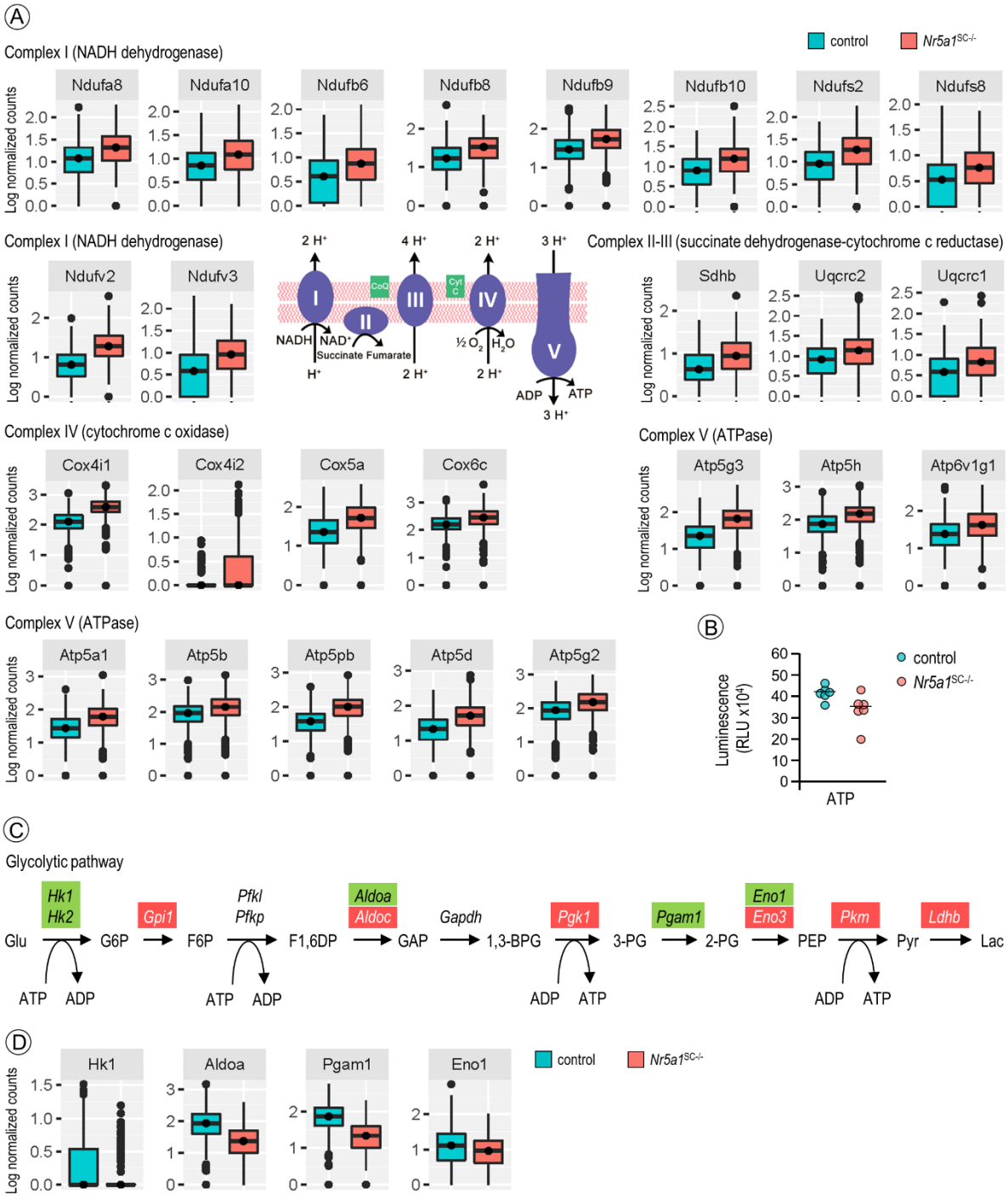

Fig. S13. ATP synthesis is not dramatically altered in NR5A1-deficient SC. (A) Tukey box plots illustrating medians, ranges and variabilities of log normalized expression of the indicated genes belonging to NADH dehydrogenase (complex I of respiratory chain), succinate dehydrogenase (complex II), cytochrome c reductase (complex III), cytochrome c oxidase (complex IV) and ATPase (complex V) in SC of control (blue boxes) and *Nr5a1*$^{SC-/-}$ (pink boxes) testes. A scheme of the respiratory chain is also depicted. (B) ATP quantities measured in of FACS-purified control (blue dots, n =6 batches) and NR5A1-deficient (pink dots, n =6 batches) SC. RLU, relative luminescence units. The difference is not statistically significant. (C) Intermediate metabolites and genes involved in the glycolytic pathway. Genes that were up-regulated and down-regulated in SC from *Nr5a1*$^{SC-/-}$ testes are indicated by red and green boxes, respectively. (D) Tukey box plots

illustrating medians, ranges and variabilities of log normalized expression of the genes harbouring a NR5A1-reposnive element (Baba et al., 2014) in SC of control (blue boxes) and *Nr5a1*$^{SC-/-}$ (pink boxes) testes. Legend:.1,3-BPG, 1,3-bisphospho-glycerate; 2-PG, 2-phosphoglycerate; 3-PG, 3-phospho-glycerate; ADP Adenosine-5'-diphosphate; ATP, Adenosine-5'-triphosphate; *Aldoa*, aldolase A; *Aldoc*, aldolase C; CoQ, coenzyme Q (ubiquinon); CytC, cytochrome C; *Eno1* and *Eno3*, enolase 1 and 2; F6P, fructose 6-phosphate; F1,6DP, fructose 1,6-bisphosphate; G6P, glucose 6-phosphate; GAP, glyceraldehyde 3-phosphate; *Gapdh*, Glyceraldehyde 3-phosphate dehydrogenase; Glu, glucose; *Gpi1*, phosphoglucose isomerase 1; *Hk1* and *Hk2*, hexokinase 1 and 2; *Ldhb*, lactate dehydrogenase B;.PEP, phospho-enolpyruvate; *Pfkl*, liver phosphofructokinase; *Pfkp*, platelet phosphofructokinase; *Pgam1*, phosphoglycerate mutase 1; *Pgk1*, phosphoglycerate kinase 1; *Pkm*, muscle pyruvate kinase.

Development • Supplementary information

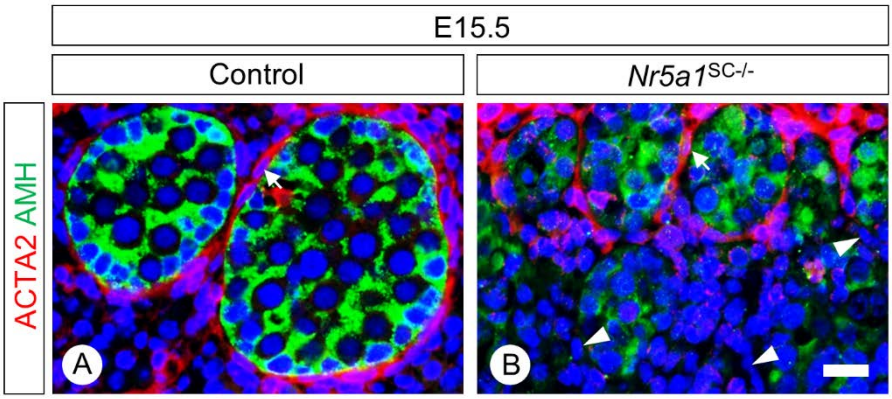

Fig. S14. Ablation of *Nr5a1* in SC impairs ACTA2 expression in peritubular myoid cells. (A-F) Detection of ACTA2 (red signal) and AMH (green signal) on histological sections of control (A) and *Nr5a1*$^{SC-/-}$ (B) testes at E15.5. Arrows point to ACTA2-positive peritubular myoid (PTM) cells, whereas arrowheads point to ACTA2-negative PTM cells. Note that ACTA2 expression is lost in PTM cells adjacent to SC where AMH expression is reduced or lost in *Nr5a1*$^{SC-/-}$ testes. Conversely, ACTA2 expression is retained in PTM cells adjacent to AMH-positive SC, which were preferentially located on the mesonephric side of the in *Nr5a1*$^{SC-/-}$ testes. Nuclei were counterstained with DAPI (blue signal). Scale bar (in B): 10 µm.

Table S1. Cluster identities

Available for download at
https://journals.biologists.com/dev/article-lookup/doi/10.1242/dev.201710#supplementary-data

Table S2. List of deregulated genes in *Nr5a1*$^{SC-/-}$ testes, categorized by cell-types

Available for download at
https://journals.biologists.com/dev/article-lookup/doi/10.1242/dev.201710#supplementary-data

Table S3. List of functional GO terms identified from deregulated genes in *Nr5a1*$^{SC-/-}$ testes, categorized by cell-types

Available for download at
https://journals.biologists.com/dev/article-lookup/doi/10.1242/dev.201710#supplementary-data

Table S4. List of anoikis-related genes (ARGs) deregulated in the *Nr5a1*$^{SC-/-}$ testis

Available for download at
https://journals.biologists.com/dev/article-lookup/doi/10.1242/dev.201710#supplementary-data

Development • Supplementary information

Table S5. Comparison of the outcome of *Nr5a1* or SC ablation during fetal development according to four distinct studies.

reference	Ikeda et al., 2021	Souali-Crepo et al., present study	Wang et al., 2020	Anamthathmakula et al., 2019
Cre line	Sox9$^{tm3(cre)Crm}$	*Plekha5*$^{Tg(AMH-cre)1Flor}$	*Plekha5*$^{Tg(AMH-cre)1Flor}$	*Tg(Amh-cre)8815Reb*
*lox*P-flanked allele	*Nr5a1*^{tm2Klp}	*Nr5a1*$^{tm1.1Ics}$	*Gt(ROSA)26Sor*$^{tm1(DTA)Jpmb}$	*Nr5a1*^{tm2Klp}
stage of Cre-mediated excision	E12.5	E13.5	E14.5	E15.5
stage of SC-death	ND	E14.5-E15.5.	E14.5	E14.5 to E15.5 (partial)
mechanism of SC-death	–	anoikis	diphtheria toxin	MDM2/TRP53-dependent apoptosis
AMH expression	lost E13.5	lost E13.5-E14.5	lost E14.5	E15.5 to E16.5
SOX9 expression	lost E13.5	lost E14.5	ND	lost E17.5-E18.5
FOXL2 expression	acquired E13.5	No	ND	ND
seminiferous cord disruption	E12.5	E14.5	E14.5	E16.5-E17.5
ECM defects	laminin lost E14.5	col-IV lost E14.5	laminin lost E14.5-E16.5	ND
fate of GC	meiotic E15.5	meiotic E14.5 dead E15.5-E16.5	dead E16-5-E18.5	dead E15.5-E18.5
fate of fetal LC	reduced number E13.5	not affected	proliferating E16.5-E18.5	not affected
fate of adult LC	–	absent	ND	ND
fate of PTM cells	ND	ACTA2 lost E15.5	ACTA2 lost E16.5-E18.5	ND
gonad at adulthood	ovary or ovotestis	testis devoid of SC and GC	ND	testis devoid of GC
Müllerian derivatives	complete tract	partial tract	ND	No

ND, not determined

Development • Supplementary information

Table S6. Primary antibodies used for immunohistochemistry experiments.

Antibodies	Species	Dilution	Source	Reference	Batch #
ALDH1A1	Rabbit polyclonal	1/50	Abcam	ab52492	GR41450-32
ALDH1A3	Rabbit polyclonal	1/20	Sigma	HPA046271	C106318
AMH	Goat polyclonal	1/100	Santa-Cruz	sc-6886	F0515
BHMT	Rabbit polyclonal	1/200	Anticorps-enligne.fr	ABIN310161	ARP41475-T100
BrdU	Rat monoclonal	1/100	Bio Rad	OBT0030S	B05D250
COL-IV	Rabbit polyclonal	1/50	Abcam	ab19808	GR3399907-2
DDX4	Rabbit polyclonal	1/2000	Abcam	ab13840	GR3317403-1
FOXL2	Goat polyclonal	1/250	Abcam	ab5096	GR181817-20
GATA 4	Goat polyclonal	1/50	Santa-Cruz	sc-1237	D3013
H2AFX	Mouse monoclonal	1/500	Millipore	05-636 (JBW301)	2506483
HSD3B1	Rabbit polyclonal	1/1000	Trans Genic's Inc	KO607	TG030317
NR2F2	Mouse monoclonal	1/200	R&D Systems	PP-H7147-00	A-2
NR5A1	Rabbit polyclonal	1/100	Cosmo Bio	KAL-KO611	TG200616
PAX8	Mouse monoclonal	1/10	Abcam	ab53490	GR3281722-12
PCP4	Rabbit polyclonal	1/500	Sigma Aldrich	HPA005792	03561
PECAM1	Goat polyclonal	1/200	R&D Systems	AF3628	YZU0122121
REC8	Rabbit monoclonal	1/200	Abcam	ab192241	GR3254930-2
SOX8	Mouse monoclonal	1/100	Novus Biologicals	H00030812-M01	07187-8G7
SOX9	Rabbit polyclonal	1/1000	Sigma Aldrich	ab5535	3677685
SOX10	Goat polyclonal	1/1000	R&D Systems	AF2864	VRY081902B
STRA8	Rabbit polyclonal	1/1000	Abcam	ab49602	GR3975217-1
TMEM184A	Rabbit polyclonal	1/200	Best et al., 2008	Best et al., 2008	not applicable
TRA98	Rat monoclonal	1/500	Abcam	ab82527	GR32800356-1
TRP53	Rabbit polyclonal	1/200	Santa-Cruz	sc-6243	A3113
TUBB3	Mouse monoclonal	1/1000	Covance	MMS-435P-0100 (TUJ1 clone)	B354040
WT1	Mouse monoclonal	1/500	Cell Marque	348M-94	31417
YFP	Chicken polyclonal	1/500	Aves	GFP-1020	GFP879484

Development • Supplementary information

Table S7. Primers used for quantification of mRNA levels by real-time RT-qPCR.

Gene	Accession number	Forward primer sequence	Reverse primer sequence	Amplicon size (bp)
Amh	NM_007445.3	5'-TCCTACATCTGGCTGAAGTGATATG-3'	5'-CAGGTGGAGGCTCTTGGAACT-3'	66
Col6a6	NM_001102607.1	5'-TGATTGCGTTCAGCAACGTG-3'	5'-TCCGGCTTGCATAGATCATAG-3'	157
Cyp26b1	NM_001177713.1	5'-CGACATCCACCGCAACAAG-3'	5'-GGCCTCCTGATATACATTGATGG-3'	151
Dhh	NM_007857.5	5'-GCACAGGATTCACTCCACTACGA-3'	5'-CCAGTGAGTTATCAGCTTTGACC-3'	172
Fst	NM_001301373.1	5'-CTGCTGCTACTCTGCCAGTT-3'	5'-ACATCCTCCTCGGTCCATGA-3'	167
Hsd17b3	NM_008291.3	5'-ATGGAGTCAAGGAGGAAAGGC-3'	5'-ATGGAGTCAAGGAGGAAAGGC-3'	76
Inhbb	NM_008381.4	5'-GCGTCTCCGAGATCATCAGC-3'	5'-CACCTTGACCCGTACCTTCC-3'	188
Itga6	NM_001277970.1	5'-GCGGCTACTTTCACTAAGGACT-3'	5'-TTCTTTTGTTCTACACGGACGA-3'	92
Pcp4	NM_008791.3	5'-GCGACCAACGGAAAAGACAA-3'	5'-TTCAGGTGGACCAGGAAGCA-3'	194
Ptgds	NM_008963.3	5'-GCTCTTCGCATGCTGTGGAT-3'	5'-GCCCCAGGAACTTGTCTTGTT-3'	118
Sox8	NM_011447.3	5'-ACCCGCATCTCCATAACGCA-3'	5'-TGGTGGCCCAGTTCAGTACC-3'	214
Sox9	NM_011448.4	5'-CAGCAAGACTCTGGGCAAG-3'	5'-TCCACGAAGGGTCTCTTCTC-3'	63
Tubb3	NM_023279.3	5'-CGTGAAGTCAGCATGAGGGA-3'	5'-TCCAAGTCCACCAGAATGGC-3'	218

Development • Supplementary information